Planetary and Space Science 102 (2014) 95–118

Contents lists available at ScienceDirect

Planetary and Space Science

journal homepage: www.elsevier.com/locate/pss

The surface geology and geomorphology of Phobos

A.T. Basilevsky [a,*], C.A. Lorenz [a], T.V. Shingareva [a], J.W. Head [b], K.R. Ramsley [b,c], A.E. Zubarev [d]

[a] Vernadsky Institute of Geochemistry and Analytical Chemistry, Russian Academy of Sciences, Moscow, Russia
[b] Department of Geological Sciences, Brown University, Box 1846, Providence, RI, USA
[c] School of Engineering, Brown University, Box D, Providence, RI, USA
[d] Moscow State University of Geodesy and Cartography (MIIGAiK), 105064 Moscow, Russia

ARTICLE INFO

Article history:
Received 3 May 2013
Received in revised form
2 March 2014
Accepted 16 April 2014
Available online 25 April 2014

Keywords:
Phobos geology
Impact craters
Grooves
Color units

ABSTRACT

The martian moon Phobos is 26 km × 22.8 km × 18.2 km in size, and the major landforms on its surface are craters and grooves. We analyzed the visible craters on the surface of Phobos where ~1300 craters ≥ 200 m in diameter, ~70 craters ≥ 1 km, and ~30 craters ≥ 2 km are identified; Stickney, the largest crater on Phobos, is about 8 km in diameter. Most craters are undoubtedly of impact origin although some small craters may be pits formed by drainage of regolith into subsurface fractures. The presence of the observed impact crater population implies that the upper hundreds of meters to a few kilometers of Phobos are heavily fractured. Using the available digital terrain model of Phobos (the dynamic version), the 24 craters larger than 2 km in diameter have been subdivided into three morphologic classes on the basis of their prominence; they are characterized by the following values of d/D ratios and maximum steepness of their inner slopes: > 0.1 and > 20°:9 craters; 0.05–0.1 and 10–20°:7 craters; and < 0.05 and < 10°:8 craters. This subpopulation of Phobos craters has a considerably larger number of craters with shallowly sloping walls compared to lunar highland craters; this may be due to several factors including the very small surface gravity of Phobos.

Most craters on Phobos are bowl-shaped, some with a complex morphology in their interiors, including concentric, flat-bottomed and with central-mounds. The size of these craters with complex morphology is indicative of layering in the target material, both regolith covering bedrock and layers within the regolith. The thickness of the regolith estimated by different techniques varies from ~5 to 100 m. Layering within the regolith does not appear to be continuous, but more lens-like. The regolith of Phobos obviously accumulated by direct crater ejecta deposition and through the return of the ejecta high-velocity fraction that escaped to near-Mars space during the impact events. The Phobos regolith may be deficient in the < 300 μm size fraction and contain martian material with concentrations ~250 ppm in the upper 0.5 m, and 1–2 orders of magnitude lower at greater depth. Downslope movement of material is revealed by downslope-trending albedo streaks and mounds on the floors and slopes of craters hundreds of meters to kilometers in size, commonly on crater inner slopes and sometimes on the outer slopes of crater rims. The albedo streaks are probably traces of geologically recent talus and avalanche emplacement. The mounds are interpreted to be landslide deposits. The different degrees of mound morphologic sharpness may be considered as an indication of their different age.

Through the geologic analysis of the MRO HiRISE color images of Stickney crater and its vicinity, we documented the distribution and mutual relations of red and blue units of the surface material of Phobos. We conclude that the red and blue "primary" materials may form relatively large blocks comprising the interior of Phobos. Crater ejecta and downslope movement of material redeposit these materials, forming secondary and tertiary derivatives of these color material units and their mixtures.

The grooves on Phobos are typically 100–200 m wide and several kilometers long and can be mapped in several intersecting systems (families) with approximately the same groove orientations within each family. They often crisscross relatively large craters, including crater rims, showing continuity with no gaps. Groove systems often intersect each other showing no lateral offsets at the intersections. At least one of groove families extends along a longitude for about 130° and this should have implications for groove formation mechanisms. Grooves similar to those on Phobos are seen on other small bodies: Eros, Lutetia and Vesta. Three different mechanisms of formation of Phobos grooves are discussed (1) grooves as fractures/faults, (2) grooves as tracks of rolling and bouncing boulders, and (3) grooves as chains of craters formed by ejecta from impact craters on Mars. The mechanism(s) of groove formation require additional studies.

* Corresponding author.

http://dx.doi.org/10.1016/j.pss.2014.04.013

We conclude that the surface of Phobos is an arena for a variety of geologic processes. The leading role belongs to impact cratering with associated target destruction, material ejection from the crater and often from Phobos, and subsequent deposition partly with temporary residence in near-martian space. Shaking by impacts and surface stirring by day-night temperature changes cause granular surface material to move down along-slope driven by very low, but nevertheless efficient, surface gravity. A sample return mission is crucially important for a better understanding of the geological processes operating on Phobos. In addition to Phobos material, a returned sample will probably contain pieces of material from Mars. A series of outstanding questions to guide future exploration is listed.

1. Introduction

Knowledge of the surface geology and geomorphology of Phobos is based on the analyses of images and other remote sensing information obtained by spacecraft. Phobos was the first small body of the solar system imaged with a resolution high enough to distinguish its surface landforms and interpret their origin with varying degrees of reliability. The first images of Phobos were received from the Mariner-9 (1971–1972) and Viking-Orbiter (1976–1980) spacecraft and these showed that the surface was dominated by craters and grooves (Duxbury, 1974; Duxbury and Veverka, 1977; Pollack et al., Noland). The dimensions of Phobos were measured with previously unachievable accuracy (Masursky et al., 1972) and using polarimetric measurements it was found that the surface is covered by "powdered" regolith with a depth of at least a few millimeters (Noland et al., 1973).

The Phobos 2 mission (Sagdeev and Zakharov, 1989) obtained results important for the understanding of the surface geology of Phobos. Based on analysis of the data taken by the ISM infrared mapping spectrometer, a spatial heterogeneity of surface spectral properties was found (Ksanfomality et al., 1989; Bibring et al., 1989; Murchie et al., 1991; Murchie, Erard, 1996). Later, the Mars Pathfinder lander on the surface of Mars obtained two spectra of the sub-Mars hemisphere of Phobos, which confirmed the surface spectral heterogeneity (Murchie et al., 1999).

The highest resolution images of some areas of the surface of Phobos (1.2–6.7 m/px) were obtained by Mars Global Surveyor. These images provided the opportunity to obtain new data on the spatial distribution of rock fragments (blocks) and their sizes, and information on the nature and distribution of mass-wasting processes (Shingareva and Kuzmin, 2001). Mars Reconnaissance Orbiter obtained several color images of Phobos using the HiRISE camera. The color images emphasize details indistinguishable or poorly seen in black-and-white images.

Between August 2004 up to 2014, the Mars-Express HRSC/SRC cameras obtained numerous images of Phobos with different resolution and supported detailed and careful study of surface morphology and geological mapping; one of the images taken by the HRSC camera with ~7 m resolution is shown in Fig. 1. Based on these data, a topographic image atlas of Phobos was created (Waehlisch et al., 2010). The size of Phobos was measured as 26 km × 22.8 km × 18.2 km (Archinal et al., 2011). Using the Doppler shift of the radio signal from Mars Express, Andert et al. (2008) determined the value of the GM product to be $0.709 \pm 0.002 \times 10^{-3}$ km^3/s^2. The bulk density of Phobos has been estimated as being in the range 1867–1885 kg/m^3 with the principal error source now being in the volume estimate (Willner et al., 2010). We describe below the results of the geological analysis of the images of the surface of Phobos, including the two major types of landforms: craters and grooves. We first consider craters, and then grooves, although in these descriptions combined considerations are sometimes unavoidable. The synthesis of these descriptions is represented in the form of a schematic geomorphic map.

2. Craters

We document the morphology of craters, crater ejecta, some aspects of crater surface density,and downslope movement of surface material on crater inner walls and crater rims. Most craters on Phobos are obviously of impact origin, although in some cases small rimless craters that could be collapse pits are observed. The majority of craters are interpreted to result from impacts by meteoroids coming from the asteroid belt, although some may be formed by impacts of ejecta from large impact craters of Mars and some small craters may be "pure" secondaries generated by impacts of the high-velocity part of ejecta from primary impact craters formed on Phobos surface, which left Phobos, orbited Mars and then intersected Phobos (Ramsley and Head, 2013a).

The surface area of Phobos is ~1200 km^2, about one-half the size of the country of Luxembourg. About 1300 craters more than 200 m in diameter were identified on images of this body (Karachevtseva et al., 2012). Of these, ~70 craters are larger than 1 km in diameter and 26 craters larger than 2 km; 17 craters on Phobos are officially named (http://planetarynames.wr.usgs.gov/). The largest crater on Phobos is Stickney, ~8 km in diameter (Fig. 1). Craters as small as 6–10 m in diameter are identified on the highest resolution images obtained by Mars Express, and the smallest craters (~3 m in diameter) were observed on the most detailed image (SP2-55103 MOC) taken by Mars Global Surveyor.

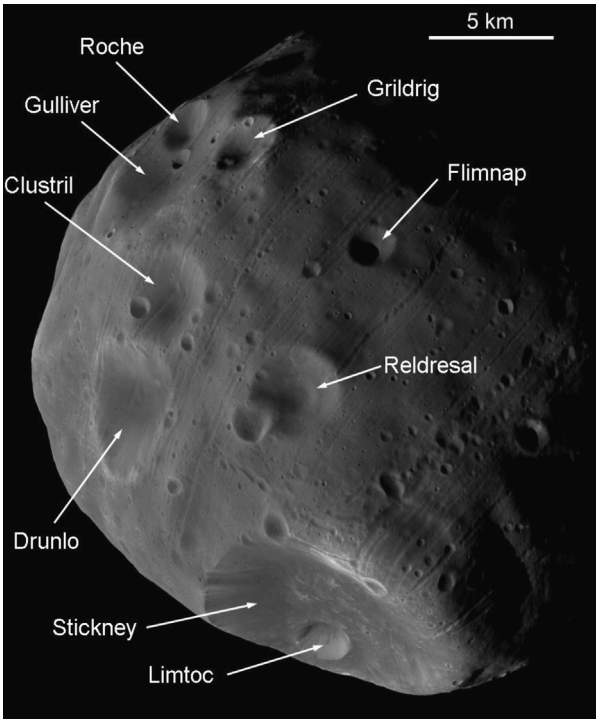

Fig. 1. HRSC image h0756 showing craters and grooves. The latter are better seen in the lower right of the image on the rim of the crater Stickney.

Comparisons with the lunar surface suggest that craters as small as decimeters and centimeters in diameter should also be present on Phobos, and impact microcraters should be present on surface rock fragments.

2.1. Crater morphology

Most craters on Phobos are simple bowl-shaped forms, often with slightly elevated rims. Their geometry can be approximated by a paraboloid of revolution or by a segment of a sphere as done earlier in the analysis of lunar craters (e.g., Florensky et al.,1972a, 1972b). Fig. 2 shows a planimetric view of the bowl-shaped craters Drunlo and Clustril (see also Fig. 1).

Smaller craters are also mostly bowl-shaped, as seen in Fig. 2. Grooves on the rims and interiors of craters are also seen; their relations with craters will be discussed later. The photogrammetric measurements involving digital terrain models (DTM) derived from the Mars-Express HRSC and SRC images (Giese et al., 2005) permitted the derivation of topographic profiles through several craters larger than 1 km in diameter within the part of Phobos covered by this DTM. Fig. 3 shows such profiles through craters Drunlo and Clustril.

These measurements showed that the steepness of the internal slopes of the morphologically prominent large craters reach 30–40°, and is locally even higher; these data indicate that the depth-diameter ratios vary from 0.15 to 0.24 (Shingareva et al., 2008). Similar results have been obtained by Willner et al. (2010).

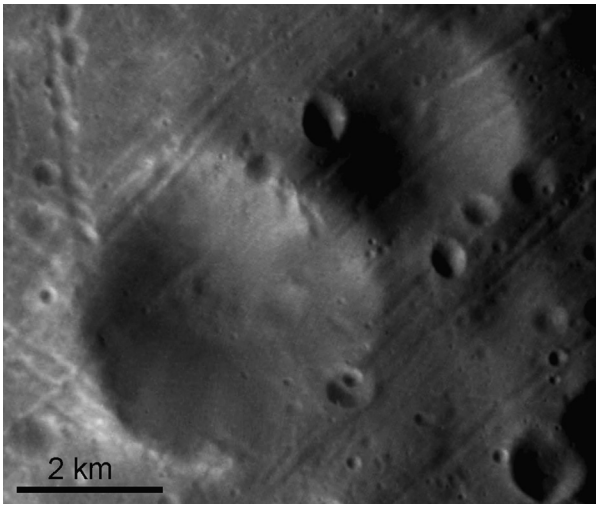

Fig. 2. Drunlo crater (lower left, 4.2 km in diameter) and Clustril crater (upper right, 3.4 km). Portion of HRSC image h2780.

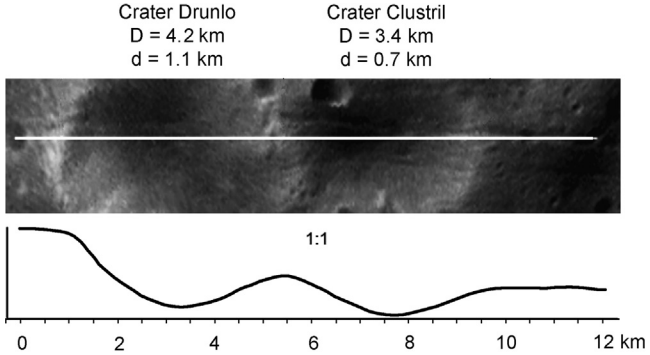

Fig. 3. Topographic profiles through Drunlo and Clustril craters. Notice that the profile line in Drunlo crater is slightly offset from the crater center.

Below we describe results of new morphometric analysis of 24 craters with diameters larger than 2 km. For that we use the new DTM of Phobos presented in two versions (Zubarev et al., 2012; Oberst et al., 2014). One version shows so-called geometric heights which are elevations above the center of the figure of this body, while another version shows the so called dynamic heights (Karachevtseva et al., in press) which are elevations above the center of the mass of Phobos corrected for gravitational attraction of Mars and the rotation of Phobos around its axis. Fig. 4 shows profiles for crater 2077 Stickney and unnamed crater 214 built for the geometric and dynamic versions of heights. Crater numbering is from the digital Catalog of Phobos craters, http://cartsrv.mexlab.ru/geoportal/. For details of the Catalog, see Karachevtseva et al. (in press). Note, each of the profiles is presented first as it was built from the DTD mentioned above, and then as rotated to make the line connecting the crater opposite rimcrests to be horizontal. The lengths of these horizontal rimcrest-to-rimcrest lines are considered as the crater diameter. The spatial resolution of the geometric version of the DTM is ~100 m, and that of the dynamic version is ~200 m.

It is seen from Fig. 4 that the general shapes of the crater profiles made in geometric and dynamic versions are rather similar. However one compares the two versions of "pre-rotational" profiles (which are "real") the inclinations of the pre-crater surfaces and the crater inner walls may be different and even inclined in opposite directions (crater 214). Taking in mind that crater formation and modification by subsequent processes occurs in the field of gravity with a significant role played by down-slope movement processes, we decided to do the subsequent analysis of the crater morphologies based on the dynamic versions of profiles.

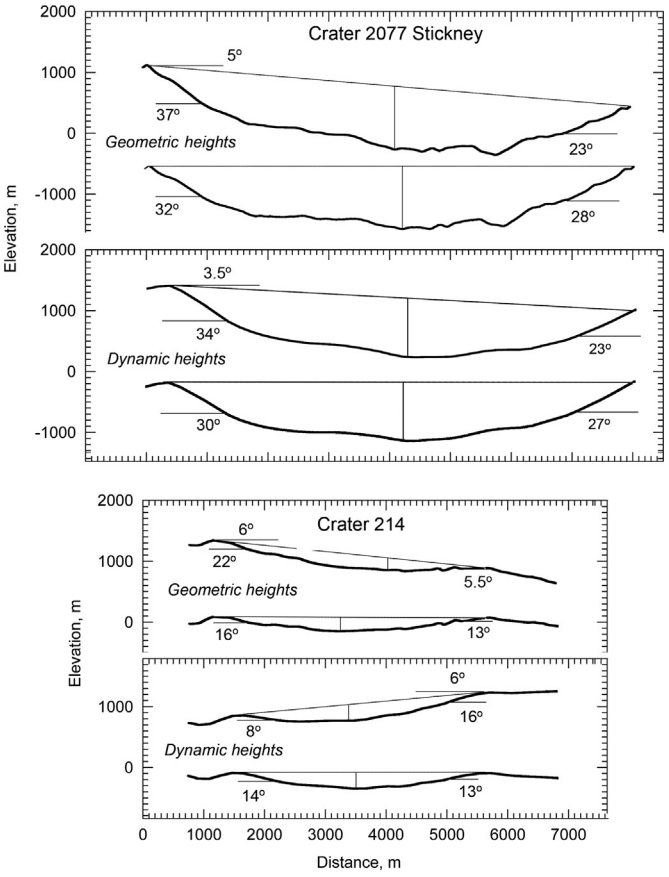

Fig. 4. Geometric and dynamic versions of profiles for craters 2077 Stickney and 214. Angles of inclination of "pre-crater" surface in relation to local horizontal plane (5°, 3.5°, 6° and 6°), as well as inclinations of the steepest parts of the crater inner slopes, are also shown.

For each of 24 craters considered, we used their "rotated" profiles to measure diameters and depths and then calculated the depth/diameter ratios. Also we measured inclinations of the steepest parts of the crater inner slopes selected by eye (see Fig. 4). Fig. 5 shows the cumulative plot for the 24 considered craters and dependence of crater depth/diameter ratios from the crater diameter.

It is seen in Fig. 5a that the cumulative function for the 24 craters has a slope close to -2, and the function $N>D=10^{4.9}\times D^{-2}$ appears to be a good approximation for the size distribution of craters on Phobos. From studies of small lunar craters, this function is well known as representing the equilibrium part of the crater population (e.g., Trask, 1966; Morris and Shoemaker, 1968; Florensky et al., 1971, 1972a, 1972b),

Fig. 5b shows that the depth/diameter ratio of the craters considered does not depend on the crater diameter. This partly resembles the characteristics of the equilibrium part of population of small lunar craters, where the approximate permanence of proportions of morphologic classes with characteristic d/D values is observed (Florensky et al., 1972a; Basilevsky, 1976).

Fig. 6 shows the dependence of the maximum steepness of the inner slopes of the 24 craters considered, on the crater depth/diameter ratio.

It is seen from Fig. 6 that the maximum steepness of inner slopes of the 24 craters of Phobos considered is in good correlation with crater depth/diameter ratios. The values of maximum steepness averaged for the opposite crater slopes are rather close to the line of dependence of these parameters found for small (20–400 m in diameter) craters in the study areas of Lunokhod 1 and 2 (Basilevsky et al., in press, Fig. 13). This suggests similarities in the processes of degradation of the craters considered on Phobos and small lunar craters.

The issue of maximum steepness and depth/diameter ratios for craters of Phobos with $D>2$ km and comparisons with these parameters of lunar craters of similar size range was earlier considered by Shingareva et al. (2008) and Kokhanov et al., (2013). Our results generally confirm their, but provide more details.

Based on our new measurements, we subdivide craters ≥ 2 km in diameter on Phobos into three morphologic classes: Class 1—those with d/D ratio >0.1, maximum steepness of their inner slope is $>20^{o}$, and may reach 40–50°; Class 2—with d/D ratio from 0.05 to 0.1, maximum steepness of their inner walls varies from 10 to 20°: and Class 3—with d/D ratio <0.05 and maximum steepness of inner wall $<10^{o}$. These three morphologic classes probably represent age categories although some special circumstances, such as shaking effects from nearby or antipodal large-scale impacts, may disturb the age versus degradation stage correlation (see e.g., Kreslavsky and Head, 2012).

According to this classification, among the studied craters of Phobos, 38% belong to class 1, 29% to class 2, and 33% to class 3. Among the lunar highland craters studied by Shingareva et al. (2008) the morphologic class distribution looks different. In their Fig. 2, depths and diameters of six Phobos craters are compared to those for 160 craters of 1–9 km in diameter from the Gagarin crater area in the lunar highlands. Morphometry data for their study were taken from Lunar Topographic Orthophotomaps. The results show that ~60% of the lunar craters considered belong to Class 1 ($d/D>0.1$), about 30% to Class 2, and less than 10% to Class 3. So, in general, the subpopulation of Phobos craters is more degraded than that in the Gagarin crater area in the lunar highlands

In interpreting this comparison, we consider three factors. The first is the irregular character of the background surface on Phobos (Fig. 1) which might favor an origin of steeper slopes at least on one side of the impact crater. However, Fig. 7 shows that this is not the case: the maximum slopes measured in 24 craters considered do not show clear correlation with the precrater surface slope. This factor certainly should play some role, but obviously seems to be minor.

The second factor may be the very low surface gravity on Phobos. The maximum steepness of crater slopes, as on any slope composed of granular materials, is obviously related to the angle of repose. This angle varies from 25° for smooth spherical particles to 45° for rough angular particles (e.g., Carrig, 1970; Pohlman et al., 2006). If the Phobos regolith is generally similar to the lunar

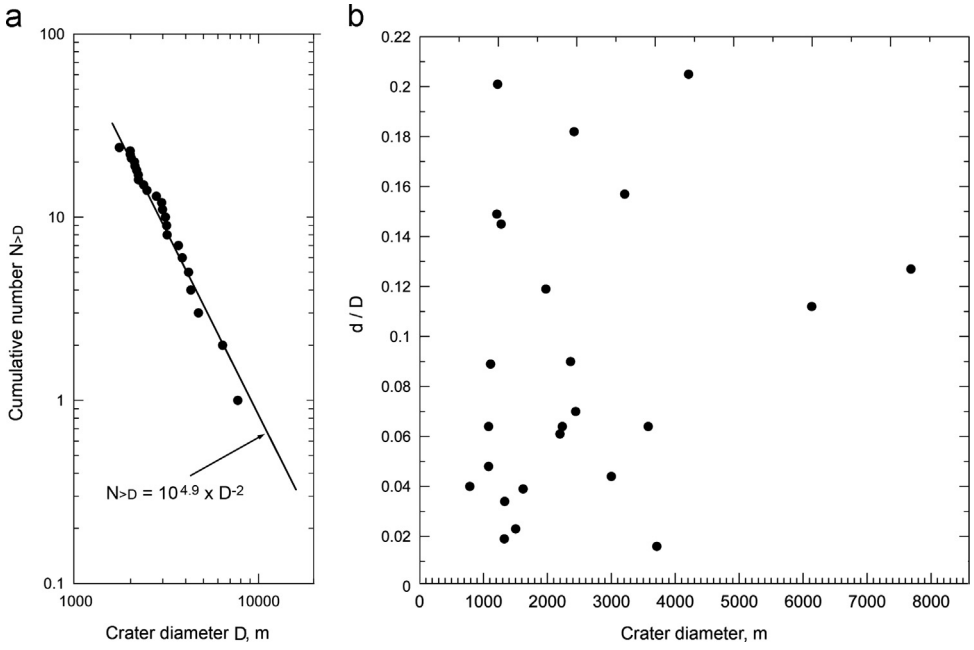

Fig. 5. (a) Cumulative plot for 24 studied craters with the superposed line of function $N>D=10^{4.9}\times D^{-2}$ (see text); (b) Plot of crater depth/diameter ratio versus crater diameter.

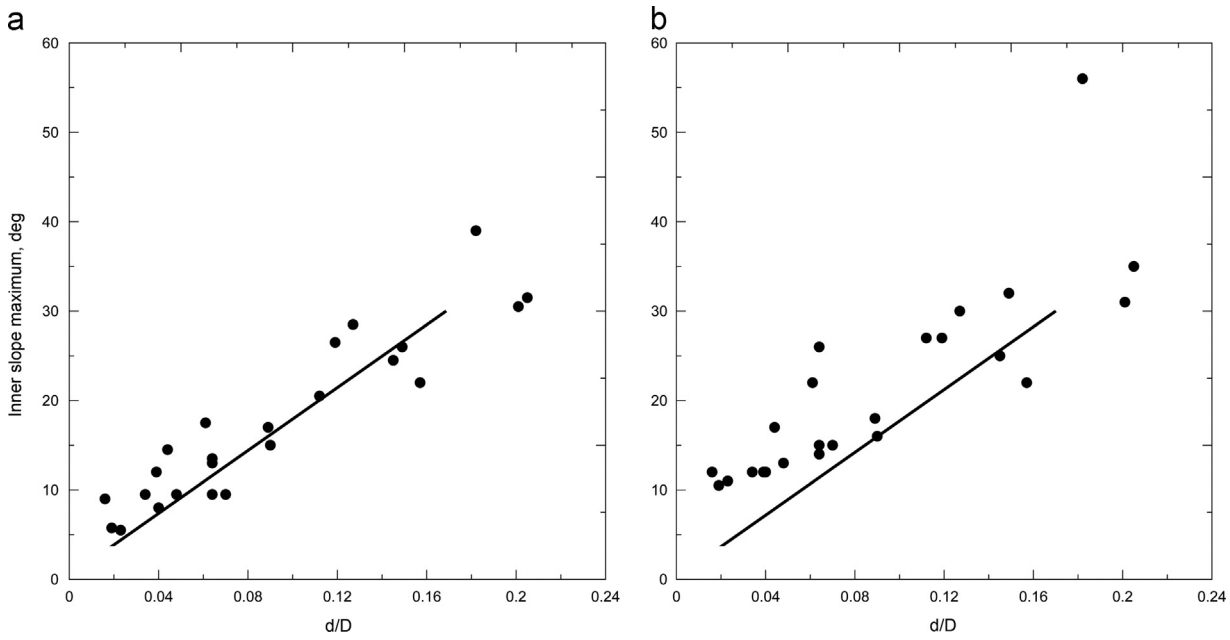

Fig. 6. Plots of maximum steepness of crater inner slopes versus depth/diameter ratios; (a) Maximum steepness averaged for the opposite crater slopes, (b) The largest values of maximum steepness. Superposed lines show the dependence of steepness of crater inner slopes on depth/diameter ratios for small lunar craters (Basilevsky et al., in press).

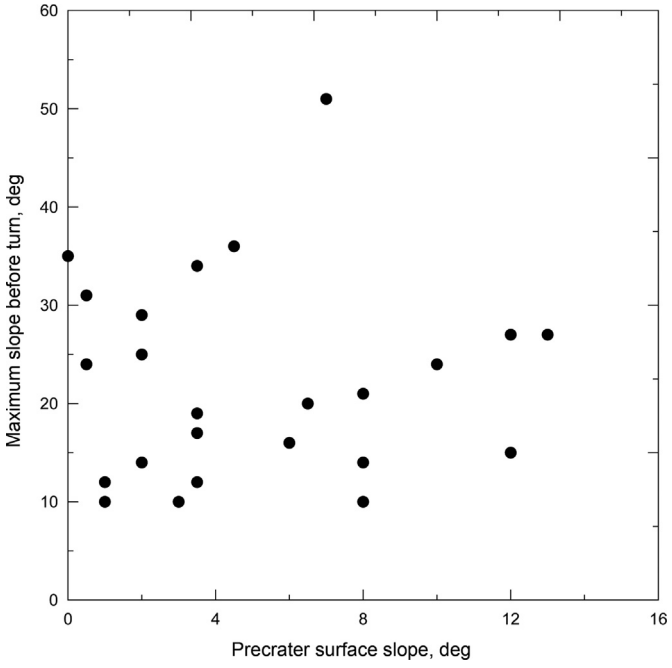

Fig. 7. Plot showing the maximum steepness of internal slopes for the profiles studied before their turn to make the rimcrest-to-rimcrest line to become horizontal versus precrater surface slope.

regolith, its angle of repose should be somewhere between these two values.

Kleinhans et al. (2011) showed that the angle of repose depends on surface gravity. In a series of experiments done in parabolic flights in a well-controlled research aircraft, avalanching of granular materials was observed in rotating drums at effective gravitational accelerations of 0.1, 0.38 and 1.0 times the terrestrial value. Granular materials start to avalanche when a static angle of repose is exceeded and then is frozen at a dynamic angle of repose. The authors extrapolated their results to the case of asteroids with $g \approx 0.02$ and concluded that its surface regolith could have static slope angles of repose up to 50° and dynamic angles of repose less than 20° for loose angular granular material. In different areas of Phobos the surface gravity varies from ~0.002 to 0.01 of the terrestrial value and this should favor the occasional occurrence of very high steepness of inner wall slopes of some craters. Shingareva et al. (2008) reported a slope as steep as 54° in the geometric type of profile and we report 51° in an unadjusted profile for crater 4745 Reldresal in the dynamic version.

The third factor playing a role in the larger portion of degraded craters > 2 km in diameter on Phobos, compared to areas of lunar highlands studied, may be the small size of Phobos which seems to enhance the shaking effects from nearby and antipodal large-scale impacts. Differences in the thickness of loose regolith layer (larger on Phobos?), the character of the subsurface material (weaker on Phobos?), and the specifics of the history of resurfacing in the Gagarin crater area in the lunar highlands also may play some role.

Only qualitative estimates exist for the morphologic prominence of craters smaller than 2 km in diameter. Thomas (1979) distinguished craters of four morphological classes: sharp, smoothed, degraded and ghost. Well-preserved (sharp), or "fresh" craters, have clear outlines, and sometimes have distinct elevated rims, and an almost pristine bowl-shaped form with rare superposed smaller craters. The smoothed craters have rather diffuse outlines and rims that are not very distinct and have smaller craters superposed on them. The degraded craters have even more diffuse outlines and have numerous smaller superposed craters. It is clearly seen that among these three classes, well-preserved craters are the deepest and have the steepest slopes, while the degraded craters are the shallowest and have the most gentle slopes. The ghost craters are barely distinguishable, close to circular, flat-floored shallow depressions, covered with many smaller superposed craters. Shingareva and Kuzmin (2008) described craters with diameters of tens to hundreds of meters as appearing similar to lunar craters of the same sizes in terms of their shapes and distribution.

Some Phobos craters display a complex interior morphology different from bowl-shaped craters: these include concentric, flat-bottomed and central-mound shapes (Thomas 1979, Thomas et al., 2000). This same range of morphologies was observed among

small lunar craters and explained by Quaide and Oberbeck (1968) as an effect of double-layer structure of the target material. In the case of the Moon the double-layer structure is caused by a loose surface regolith layer overlying mechanically strong bedrock. On the basis of laboratory experiments, they showed that if the crater is formed totally within the regolith, it produces a bowl-shape. If the depth of the crater as it forms approaches the upper boundary of the bedrock, the crater formed has a central mound. If the crater cavity penetrates only slightly into the bedrock, a flat-bottom crater is formed. And if the crater cavity deeply penetrates into the bedrock, a concentric crater with a terrace-like bench is produced. The Quaide and Oberbeck (1968) experiments showed that if one designates the crater diameter as D and the regolith thickness as L, then at $D/L < 4$, craters are bowl-shaped, at $D/L = 4–7.5$, craters have a central mound, at $D/L = 8–10$, craters are flat-floored, and at $D/L > 10$ craters are concentric.

Analyzing HRSC and SRC images, about 60 craters of complex internal morphology have been found on the surface of Phobos. All three types of craters with complex morphology were observed: flat-bottomed, containing a central-mound, and concentric (Fig. 8). Images of 34 craters have been examined at the most favorable illumination conditions. The range of diameters of craters with complex interiors is 60–3500 m. Among the craters with complex internal morphology, the concentric craters are the most broadly distributed on Phobos, while flat bottomed and central mound craters are relatively rare. In 20 cases we were able to estimate the thickness of the upper layer, which can be a layer of the total regolith or only the upper layer of regolith (Fig. 8d). The estimated thickness of the upper layer of the regolith in the observed complex craters is in the range of 1/6–1/12 of the crater diameter. The largest crater of complex morphology is the ~3500 m concentric crater Reldresal (Fig. 8c); this has a scarp on the inner slope at a depth ~400 m, measured from the crater rim crest.

The analysis showed further that a concentric morphology, which implies a layered target structure, is observed in a given crater but is not seen in neighboring craters of the same size; thus, the deduced regolith layers are unlikely to have a regional distribution. The suspected layers could be individual ejecta blankets having a different granulometric composition or lithified to varying degrees and therefore, having different mechanical strengths. As described by Thomas et al. (2000), the regolith of Phobos may have a considerable thickness, so even in kilometer-sized craters with complex morphology, the evidence for strength differences might indicate layers within the regolith, but not a basement of solid rock or solid blocks.

The external morphology of craters more than 200 m in diameter also shows some variability. A relatively small number of craters are of elliptical shape (Fig. 9a). They probably formed by

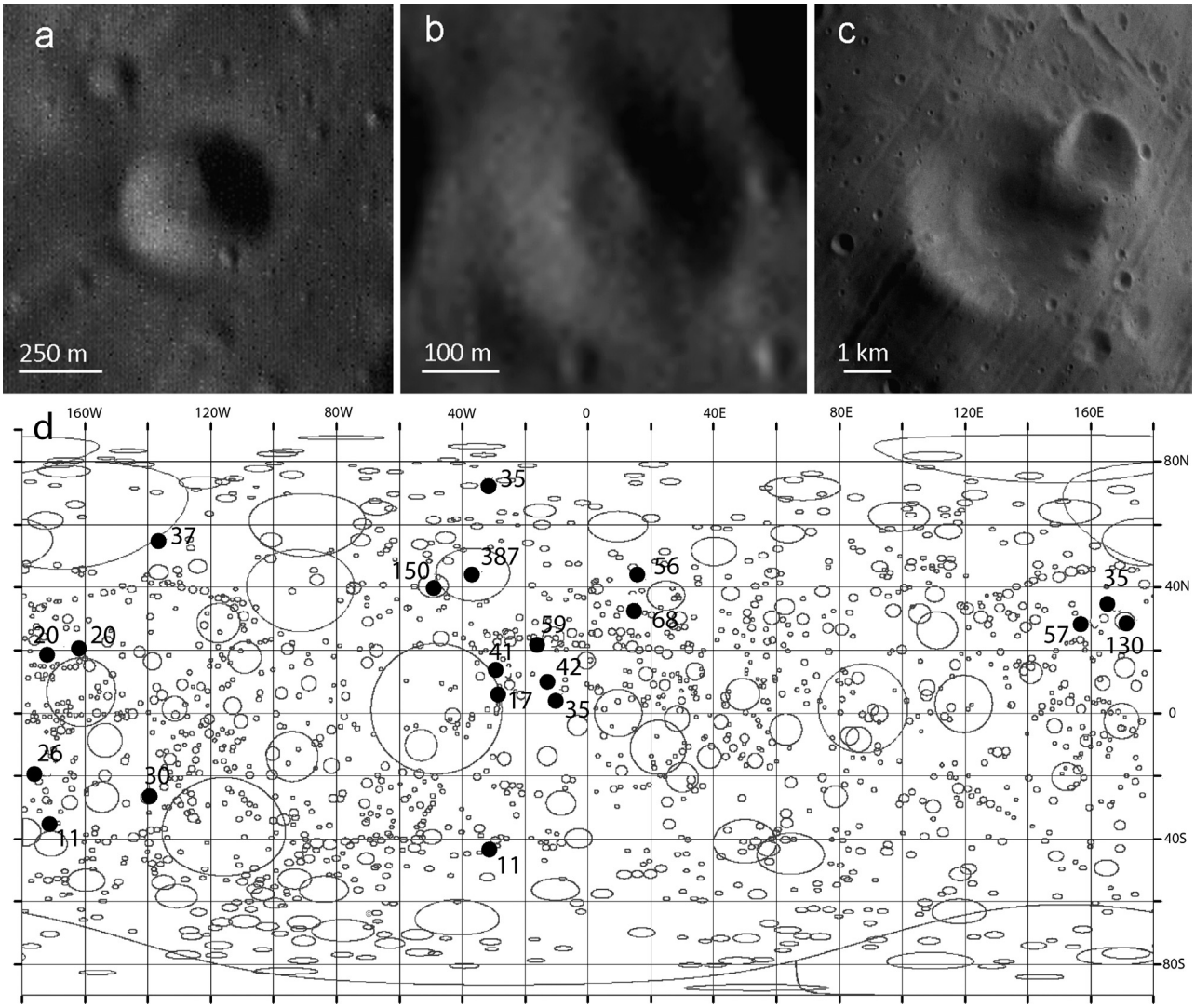

Fig. 8. (a) Flat-bottomed crater (D~480 m), (b) Central-mound crater (D~350 m), (c) Concentric crater Reldresal (D~2.9 km). Portions of HRSC image h0756 and (d) Map of estimated thickness (in meters) of the upper layer. Background represents data from digital Catalog of Phobos craters, http://cartsrv.mexlab.ru/geoportal/.

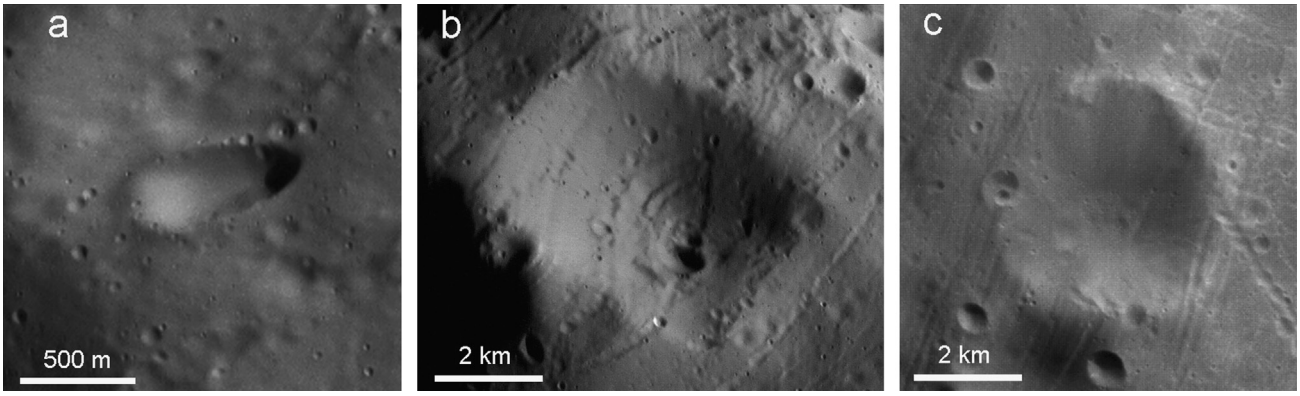

Fig. 9. (a) A 750 × 250 m elliptic crater, (b) Hall crater, 6.2 km in diameter, (c) the 4.6 km crater Drunlo; portions of HRSC images h8974, h9574 and h2780 respectively.

oblique impacts of meteoroids, ejecta of craters of Mars, and some could be secondaries formed by high-velocity ejecta from primary craters on Phobos that orbited around Mars and subsequently collided with Phobos.

Some craters are characterized by polygonal planimetric outlines. The square-shaped crater Hall (Fig. 9b) has two mutually opposite linear rim segments coinciding with undulations of the background surface and two linear segments approximately perpendicular to them, in turn being parallel to the system of grooves. Planimetric outlines of the 4.6 km crater Drunlo (Fig. 9c) show some triangularity, two directions of which coincide with the systems of grooves. The crater could be formed originally as polygonal due to an appropriate structural pattern of the target, and could also become polygonal due to degradation processes: superposition of other craters, subsequent formation of grooves and down-slope mass-wasting. In some cases elements of polygonality may be apparent (see, for example, the left rim of Drunlo crater in Fig. 9c).

2.2. Crater ejecta and regolith

The formation of regolith on Phobos should generally be similar to that on the Moon and asteroids and include such multiscale, multistage and repeating processes as impact fragmentation and melting of target materials, cratering with excavation of target materials from different depths and mixing, lateral transportation with high-velocity portions leaving Phobos and partial re-accretion of the latter back to Phobos surface (see Ramsley and Head, 2013a). Space weathering of the materials exposed to solar and space radiation is also an inevitable part of the process. As a result, the surface of Phobos should be covered by an unsorted mixture of fragments of solid rock and impact melt of different sizes in a range from micrometers to meters. The subsurface layers could contain the same material, including portions lithified to various degrees due to impact-induced compaction and thermal metamorphism similar to that known in lunar samples and meteoritic regolith breccias, coming to the Earth from asteroids and the Moon.

The gravitational field of Phobos is low due to small size of this body and is highly heterogeneous due to its irregular shape, so the escape velocity from the surface of Phobos is highly variable. According to calculations by Davis et al. (1981) for a model of a three-axis ellipsoid, the escape velocity is 10.5–15.5 m/s at the poles, 3.5–13 m/s at the sub-martian point and is widely varying along the equator. Because of the low escape velocities, the effect of the rotation of Phobos around its axis should noticeably affect the pattern of crater ejecta escape, making it asymmetric, especially in places close to the equator of this body. According to estimations by Thomas (1993), the low velocity (typically 4–6 m/s) crater ejecta should form relatively narrow asymmetric blankets around the craters, while the high-velocity material transfers to martian orbit (see also Wilson and Head, 2014). For Stickney crater ejecta, this asymmetry should result in the escape velocity being ~2.4 m/s to the east and ~9.8 m/s to west from the crater (Thomas, 1998). In the Viking-Orbiter image of Phobos, a triangle-shaped area with hummocky relief is clearly seen to the east of Stickney. Thomas (1998) interpreted this area as an asymmetric ejecta blanket from Stickney. However, Shingareva and Kuzmin (2001) provided evidence supporting an alternative interpretation of the formation of this hummocky terrain as a result of landsliding inside Stickney crater and emplacement of part of the landslide out onto the crater rim.

Prominent ejecta deposits around Phobos craters are not often observed. Fig. 10 shows a few examples of these.

Fig. 10a shows a 150-m diameter crater surrounded by bright ejecta with a rayed structure. The high albedo of lunar crater rays is usually explained by the differences in maturity (less mature) and/or composition (more feldspatic) between the materials of the ejecta and surrounding area (Hawke et al., 2004). The same factors could be acting in the case of crater rays on Phobos. For simple impact craters, the maximum depth of excavation is typically 0.15–0.2 of the crater diameter (e.g., Horz et al., 1991). Applying the estimated depth of excavation as a function of crater diameter, one can conclude that the bright material here occurs at some depth down to 20–30 m below the surface.

Fig. 10b shows a 45-m diameter crater surrounded by bright ejecta surrounded by the light halo. As discussed above, the brighter ejecta and halo can be explained by the differences in maturity and/or composition between the materials of the ejecta and surrounding area. Applying the estimated depth of excavation as a function of crater diameter, one can conclude that the brighter material here occurs at some depth down to 7–10 m below the surface.

Fig. 10c shows a 20-m diameter crater surrounded by a bright ejecta deposit, which in turn is surrounded by a relatively dark halo. Such a concentric ejecta pattern may suggest a two-layer structure of the regolith material in this place. The upper layer material is relatively dark while the underlying material is relatively bright. The nature of the dark material ejected from the craters is not known. It could be fragmented impact melt from pre-existing craters that forms a part of the regolith, or carbon-rich regolith material like carbonaceous chondrites (Pronin and Nikolaeva, 1982). Typically, in the impact cratering process, the material in the zone where impact melt forms, becomes the high-velocity part of the crater ejecta (Basilevsky et al., 1983; Melosh, 1989). So in the case of Phobos, where escape velocities are very low, impact melt should typically leave the body and not form concentrated accumulations. Thus, in the dark haloes of Phobos

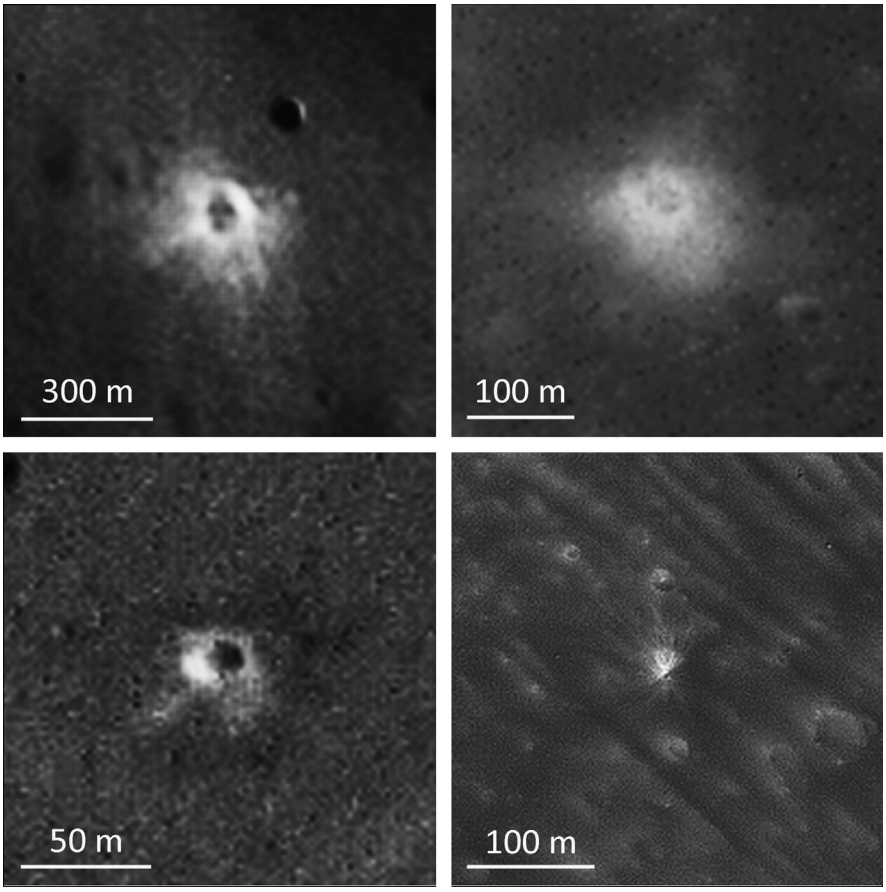

Fig. 10. Ejecta from craters on Phobos; (a) Bright ejecta with a rayed structure around a 150-m crater. (b) Bright ejecta surrounded by light halo around a 45-m crater. (c) Bright ejecta surrounded by dark halo around a 20-m crater. (d) Bright rays around a crater ~5 m in diameter; images VO2_246a68, VO2_246a68, h8974_0000.nd2 and PSP_007769_9010_RED, respectively.

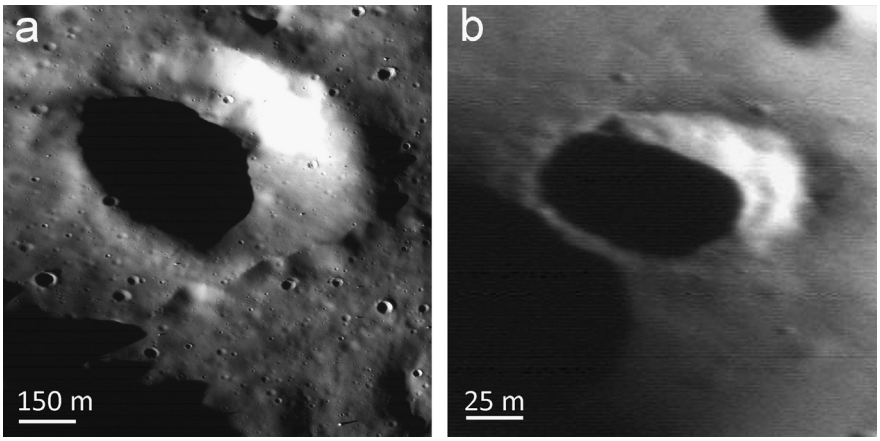

Fig. 11. Examples of craters on Phobos with "lobes" on the distal ends of their ejecta deposits; (a) Oblique view of a 700 m crater, (b) Oblique view of a 100 m crater; portions of MGS image 55103.

craters, a carbonaceous dark material seems to be more probable, relative to fragmented impact melt. Applying the estimated depth of excavation, one might conclude that the brighter material occurs at a few meters depth with the dark material above it. Alternatively, the bright material may simply be immature, and thus the same composition as the darker layer (see Pieters et al., 2013, for further discussion).

Fig. 10d shows a 5-m diameter crater surrounded by rays of bright ejecta superposed on the relatively dark surface. Again, applying the estimated depth of excavation one might conclude that the bright material here occurs at a depth of less than one meter, with dark material above it.

It is necessary to note that by using the terms bright and dark we mean relatively bright and relatively dark. The observed differences in brightness of these materials are certainly emphasized by image processing and in reality may be minor, but their observations are important as evidence of differences in composition and maturity. The cases described could mean that brighter and darker, finer and coarser, immature and mature materials occur at various depths, from meters to hundreds of meters.

If true, these are probably not laterally continuous layers but discontinuous lenses.

Rays associated with some craters of Phobos strongly resemble rays associated with small lunar craters (e.g., North Ray and South Ray craters at the Apollo 16 landing site, Muehlberger et al., 1972). The origin of the rays seems to be due to interaction between an impact-induced shock wave in a target and nonuniformities of target properties, including target relief (e.g., Shuvalov, 2012). The Phobos craters with rays, like their lunar analogs, seem to be relatively young features but quantitative estimates of the ages of rayed crater is not yet completely reliable, even for lunar features (e.g., Honda et al., 2011).

Some craters on Phobos have ejecta deposits (Fig. 11) whose distal ends remotely resemble lobes of Martian rampart craters with fluidized ejecta (Carr et al., 1977; Squyres et al., 1992).

This, if true, could indicate the presence of water ice in the subsurface layers of Phobos. Theoretical models suggest that if Phobos contained water ice early in its history, it is possible that this ice-containing material might still remain at depths 270–740 m at the equator, and at tens of meters at higher latitudes (Fanale and Salvail, 1990). However, the observed intensive impact reworking of the Phobos surface leaves little possibility for the occurrence of ice close to the present surface. Thus, a better planetary analog for Phobos crater lobate ejecta may be ejecta of the lunar King crater that displays prominent flow features (El-Baz, 1972; Howard, 1972). In both martian and lunar cases the ejecta lobes are obviously deceleration lobes and there may be similar features that can be produced in the Phobos environment.

The minimal thickness of impact ejecta deposits for the craters of different diameters on Phobos, estimated by Veverka et al. (1986) based on theoretical model of impact crater formation by Housen et al. (1983), is 2 m; the maximal thickness is 100 m, and the average thickness is 35 m. As estimated by Thomas (1998), the thickness of Stickney crater impact ejecta decreases from 100 m in the eastern part of crater rim to 20 m in the western part. The minimal regolith thickness estimated by morphological features of Phobos craters and grooves is ~5 m, and the maximum is ~100 m (Thomas et al., 2000).

2.3. Blocks and boulders

Blocks and boulders – large pieces of solid rock – are also observed on the surface of Phobos (Fig. 12) and as on the Moon are thought to be a result of impact cratering of this body. They were first recognized on the images taken by the Viking-Orbiter (Thomas, 1979). The smallest blocks observed then were ~15–30 m in diameter. The largest one, observed inside Stickney crater, was ~100 m across (Thomas, 1979). The boulders have isometric or slightly elongated shapes and in some places are grouped into clusters. The boulders were interpreted as possible fragments of primary basement rocks and/or impact-generated solid rocks (impactites) ejected from large craters (Thomas, 1979).

Fig. 12 shows an area on Phobos with numerous boulders. On the left of the figure is a map of the areal distribution of rock boulders from Thomas et al. (2000). On the right side is an image of one of subareas of this part of the surface of Phobos. Craters of a few meters to 200 m in diameter are seen and show different morphologic degradation states ranging from very subdued, to sharp ones with elevated rims and shadows inside. Fig. 12 shows

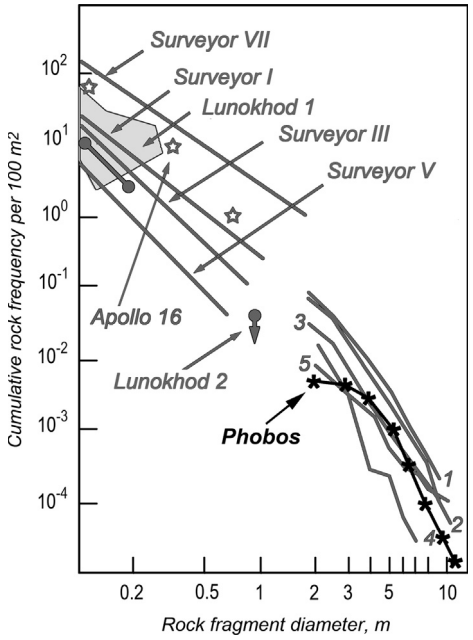

Fig. 13. Cumulative frequency of rock fragments on the surface of Phobos in comparison with the rock fragment frequency on the lunar surface; 1—lunar highland, 2—Aristarchus Plateau, 3—Mare Imbrium (area of Lunokhod 1 studies), 4—Oceanus Procellarum, 5—Sinus Medii. The data are from: Surveyor – Shoemaker and Morris, 1969; Apollo 16—Muehlberger et al., 1972; Lunokhod 1—Florensky et al., 1971, 1972b, 1978; Lunokhod 2 - Florensky et al., 1976;

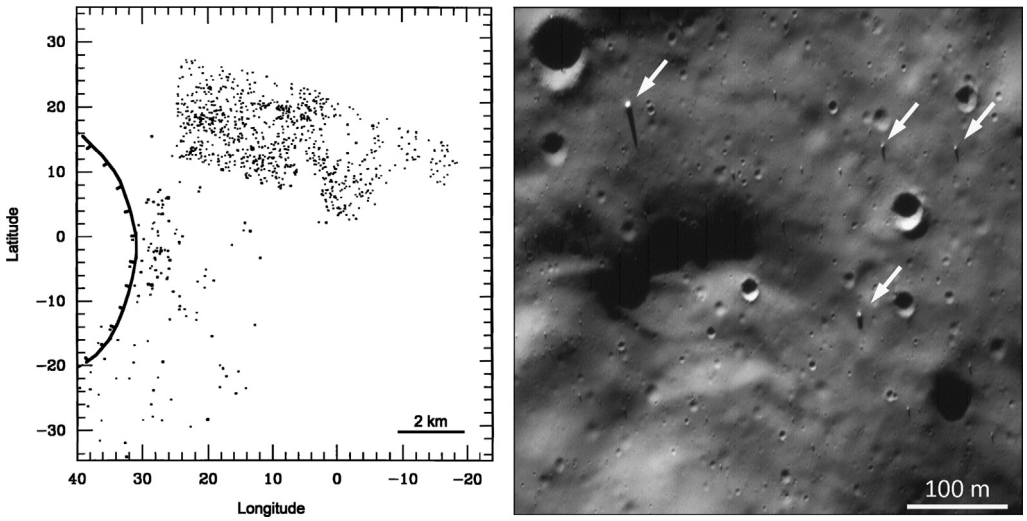

Fig. 12. (a) Area east of Stickney crater with numerous boulders of a few to 85 m in diameter (modified from Fig. 5 of Thomas et al. (2000)). (b) Boulders a few meters in diameter on the surface of Phobos. Portion of MGS image 55103.

part of a broader area characterized by the high-resolution images (~2–7 m/px) taken by Mars Global Surveyor in 1998. It covers Stickney crater and the terrain to the east of it, including the sub-martian point. Using these images, the size and spatial distribution of blocks reliably identified on the surface of Phobos was studied (Thomas et al., 2000). The largest identified block was ~85 m in diameter. Based on analyses of these images Thomas et al. (2000) suggested that most of large blocks are related to Stickney. However, the nature of this relation is unclear. Stickney appears to be a rather old landform on the basis of its morphologic state of freshness. Based on the density of superposed small impact craters, its age was estimated to be ~3.5 to 4.2 Ga (see section 1.3 below), while the time of survival of meter-sized boulders based on analogies with the time of survival of lunar rocks is a few hundreds of millions of years (Basilevsky et al., 2013).

Shingareva and Kuzmin (2001) counted less visually prominent meter-sized bumps that were interpreted as blocks, covered by regolith or partly destroyed by micrometeorite impacts. Their number was found to be two times larger than the number of blocks counted by Thomas et al. (2000) on the most detailed high resolution MGS image 55103 (centered at 28.61°N, 20.16° W). The meter-sized blocks are rather chaotically distributed on crater rims and around small craters, occasionally forming small chains and clusters (Shingareva and Kuzmin, 2001).

Fig. 13 shows the cumulative frequency of rock fragments as a function of their diameter given by Karachevtseva et al., in press in comparison with the frequency of rock fragments determined by different missions to the Moon. In the ~16 km^2 area on MGS image 55103, ~900 rock fragments ranging from 2–16 m in diameter were counted. The study area is within 5°S-22°N, 17°W-30°E, and this includes the sub-martian point on the surface of Phobos. 1–3 unpublished data by E.N. Slyuta; 4, 5 – Florensky et al., 1972a.

It is seen in Fig. 13 that the size frequency distribution of the rock fragments in the study area on Phobos is within the range of values typical for rock fragments of the same sizes on the lunar surface. It is difficult to say if the study area is representative of the surface of Phobos, in the sense of the areal distribution of rock fragments, but one important implication can be deduced from this observation.

Because Phobos is so close to Mars, the gravity field on its surface in addition to proper Phobos gravity has a tangential component due to the martian gravity field and oriented toward the sub-martian and anti-martian points (Davis et al., 1981). Depending on the value of the tangential component and local topography with respect to the equipotential surface, movement of material toward these points on the slopes are slightly preferred and may have a regional trend. The actual effectiveness of this phenomenon is not clear and requires additional studies. In the case of sub-martian point, however, some assessment (probably also applicable to the anti-martian point) can be currently undertaken: the surface characteristics of the area close to sub-martian point, such as the presence of morphologically sharp landforms and blocks of rocks (Figs. 10 and 11, see also Fig. 9 in Thomas et al., 2000) seem to imply no substantial supply of material from other areas of Phobos trending towards the sub-martian point. Therefore, the predicted trend is not clearly observed on the local scale if it exists at all.

It would be interesting to make a global survey of the areal distribution and the size distribution of rocks fragments on Phobos. However, except for the area covered by MGS image 55103 mentioned above, the resolution of images of the surface of Phobos is certainly not enough for reliable results: Only ~30% of Phobos' surface is covered by images with resolution 3–6 m, another 30% covered with resolution 6–10 m and the rest ~40% – with resolution 10–20 m (Karachevtseva et al., in press). Taking in mind that for reliable identification of any feature it should be covered at least by 3, but better 5 pixels, it is obvious that the global survey is possible only for rocks fragments larger than 20–50 m in diameter, which are very rare.

2.4. Crater density

The issue of crater density is generally covered in the paper "Surface chronology of Phobos: The age of Phobos and its largest crater, Stickney" by Schmedemann et al. (2014). Here we add only several notes on this topic. The analysis of Viking-Orbiter images showed that the spatial density of craters on the surface of Phobos is close to that on the ancient surface of the lunar highlands (Thomas and Veverka, 1980). The crater population on Phobos is considered as being close to an equilibrium state, a state at which a further increase in crater density is impossible due to the fact that each time a new crater is formed, a previously formed one is destroyed (see also our Fig. 5). According to Thomas and Veverka (1980) the density of craters >1 km in diameter is close to the limit of possibility for a small body the size of Phobos, since an increase in density of such craters by one-third would destroy the whole body. Estimations of crater density performed in various regions of Phobos did not reveal areas in which the density differed from the average by more than a factor of two. This suggests that on Phobos there are no extended areas that are significantly younger or older than most of the surface (Thomas and Veverka, 1980).

The paper by Schmedemann et al. (2014) is based on crater counts within the 177 km^2 area west of Stickney crater, considered to be a good representative of the average surface of Phobos, and two partly overlapping areas inside Stickney crater: 25 and 10 km^2. For estimations of the crater retention age Schmedemann et al. (2014) used two chronology functions: one assuming that Phobos has been in its current orbit about Mars since its formation (case A), and another assuming the recent capture of Phobos and the impact history of an average main asteroid belt (case B). The crater counting results suggest that the age of an average surface of Phobos is about 4.3 Ga (Case A) or 3.66 Ga (Case B). The Stickney age was determined to be ~4.18 Ga (Case A) or 3.54 Ga (Case B).

However Ramsley and Head (2014) proposed a hypothesis suggesting that age of Stickney may be much younger than it was found by Schmedemann et al. (2014). They show in their model that the high-velocity ejecta generated by the Stickney-forming impact, after these ejecta went into orbit around Mars, could re-impact onto Phobos, producing secondary craters which would result in a bias toward an older date for Stickney. More studies including analysis of morphologies of small craters in the vicinities of Stickney and more sophisticated modeling are necessary to resolve this problem.

Robinson et al. (2003) found that an undersaturated distribution of craters smaller than 200 m in diameter is common for Phobos, Eros and the Moon, and proposed that downslope motion of material could erase the craters formed in relatively thick regolith. In considering these data, one should take into account (as shown for the case of Phobos by Shingareva et al. (2008) that the identification of small craters is very sensitive to illumination conditions: if the Sun is high above the horizon, then some degraded and ghost craters lose their visibility. If the Sun is very low, there are extended shadowed areas on the rough background surface of Phobos, within which small craters are not visible. The optimum for crater identification, and thus crater counts, is when the Sun is 15–20° above the horizon (Shingareva et al., 2008). In summary, the undersaturated distribution described by Robinson et al. (2003) may be an influenced by illumination geometry.

2.5. Downslope material movement

The first evidence of downslope movement of material on Phobos was described by Thomas (1979) on images taken by Mariner-9 and Viking orbiters; they described downslope-trending narrow albedo streaks on the inner walls of some craters. Since that time new missions have provided more observations suggesting that despite the very minor surface gravity (≤ 0.001 that of Earth), downslope movement of regolith material is rather typical for Phobos (e.g., Thomas, 1993; Shkuratov et al., 1991; Thomas, 1998; Shingareva and Kuzmin, 2001). Figs. 14 and 15 show several examples of the features suggesting downslope material movement on the surface of Phobos.

Fig. 14a shows albedo streaks on the inner slopes of the largest crater on Phobos, Stickney ($D \approx 8$ km) and the smaller crater Limtoc (~2 km), while Fig. 14b shows similar albedo streaks on the inner slopes of Todd crater (2.6 km). The streaks of slightly brighter and darker material trend downslope, and are probably components of granulated talus material. Variations in the streak brightness are probably due to either brightness variations of the source materials for each given streak, or differences in optical maturity, as discussed earlier concerning the brighter and darker

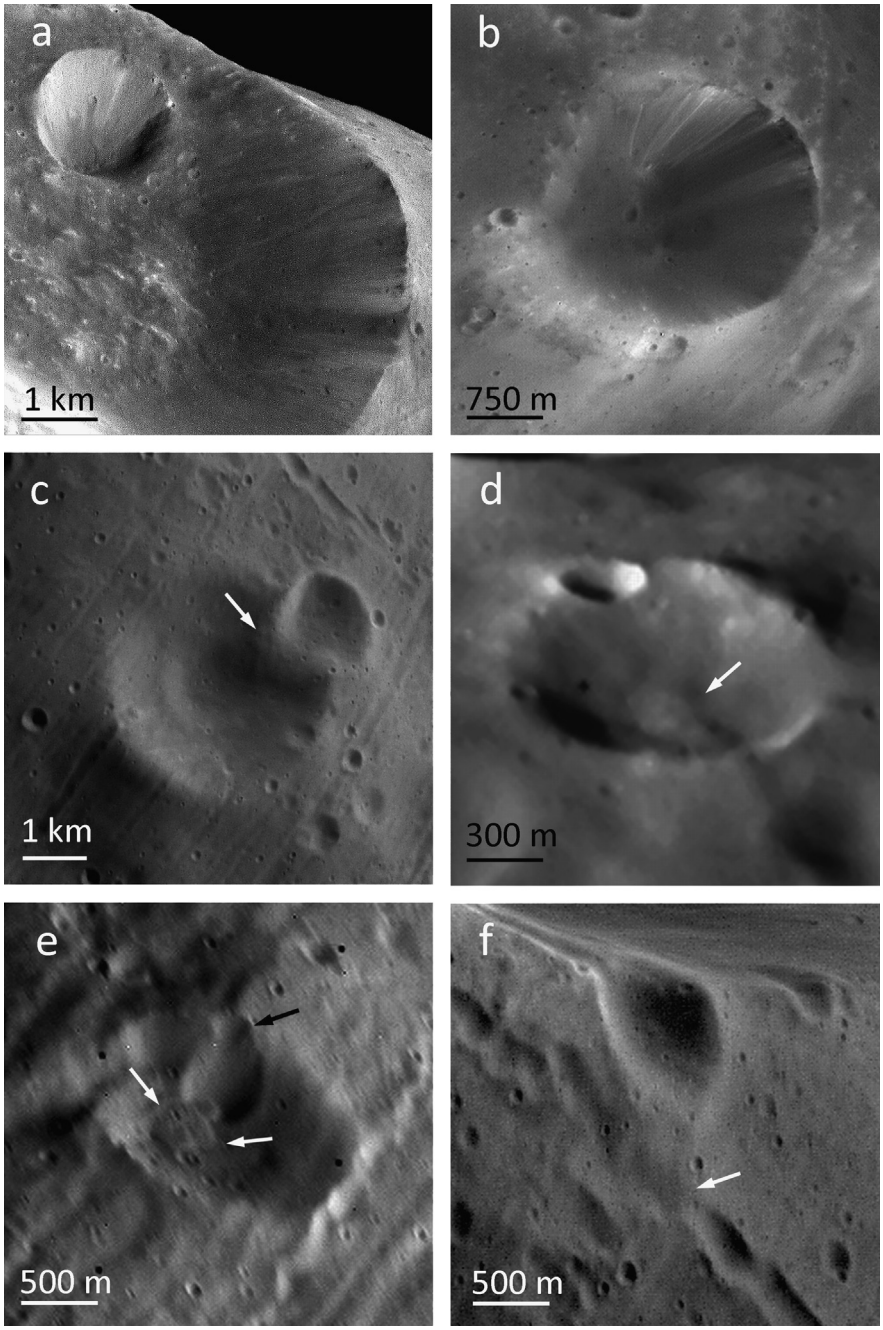

Fig. 14. Examples of downslope material movement. (a) Albedo streaks on the inner slopes of Stickney and Limtoc craters and the hummocky floor of Stickney crater, probably a landslide deposit; portion of HRSC image h0756_0000.p22. (b) Albedo streaks on the inner slopes of Todd crater; HRSC h0756_0000.p12. (c) Absence of observed grooves in the NW and SE segments of the inner slopes of Reldresal crater and the mound of a body of regolith that has slid (arrow) in the Reldresal NE segment; potion of HRSC image h0756_0000_s22. d) Landslide (arrow) on the floor of a 1.4 km crater; portion of VO1 image 343a15. (e) Landslide (white arrows) on the floor of a 1.3 km crater caused by a 200-m crater (black arrow) that formed on the rim; portion of VO1 image 243a71. (f) Rim of a 1.5 km crater that has apparently slid downslope, covering the nearby groove (arrow); portion of HRSC image h0756_0000.p12.

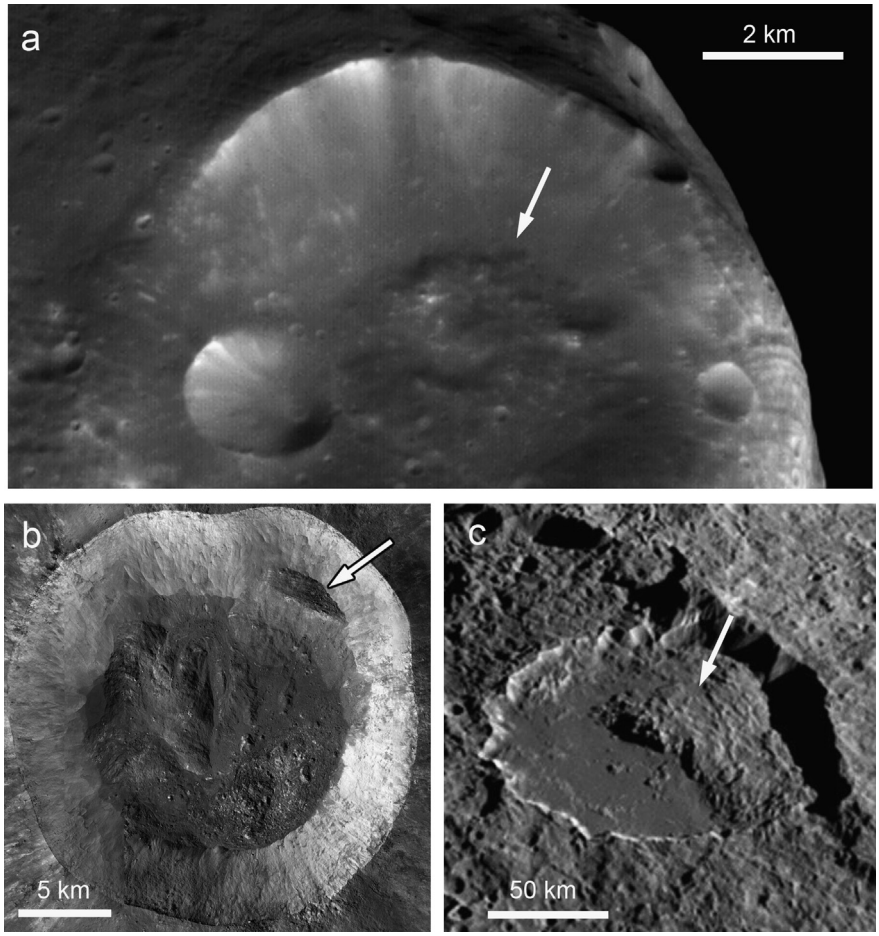

Fig. 15. Examples of hummocky terrain of the landslide deposits on the floors of impact craters. (a) Hummocky terrain (arrow) on the floor of Phobos crater Stickney; portions of HRSC image h4340_0000_s.22; (b) Hummocky floor and landslide terrace (arrow) on the slope of the lunar crater Giordano Bruno; mosaic of LROC NAC images M185212646LR, M185219795LR, M185226944, M185234092; (c) Hummocky surface of the giant landslide (arrow) in the Iapetus crater Malun; Cassini ISS image PIA06171.

ejecta of craters on Phobos (see Fig. 10). The presence of the streaks on the slopes has certain age implications. Due to impact reworking of the surface of Phobos, streaks eventually have to be destroyed, so the fact that we see them suggests their youth or renewal. Shevchenko et al. (2012) recently described a rather similar phenomenon on lunar crater slopes. Using a combination of spectrophotometric studies and ages of exposed lunar materials, they estimated that the lower limit of the age of the downslope material movement described by them was 40–80 years. These estimates obviously cannot be directly translated to Phobos downslope streaks, but they certainly support the conclusion as to their youth. The hummocky floor of Stickney crater is probably a landslide deposit (see below, Fig. 15).

Fig. 14c shows Reldresal crater (2.9 km), around which and on its rim are seen grooves. The latter are not observed, however, on the inner slopes of this crater; the inner slopes appear almost featureless. This suggests that the slope surface is covered by a mantle of granulated material slowly moving downslope by a creep mechanism activated by the day/night temperature changes of the surface layer as well as by seismic shaking and impacts due to meteorite/micrometeorite bombardment. A 1.5-km crater is superposed on the NE segment of Redresal crater. The SE segment of this crater rim forms a concentric mound intruding on the inner slope of Reldresal crater.

Fig. 14d shows a 1.4 km crater with an apparent landslide on its floor. The subdued outlines of the landslide suggest that it has a relatively old age. Fig. 14e, on the contrary, shows a rather young landslide with sharp outlines. It occurs on the floor of a 1.3 km crater and its formation was probably caused by impact on its northern rim, which formed a 200-m crater. Fig. 14f shows a landslide formed due to collapse of the southern rim of a 1.5 km crater. The landslide overlapped the neighboring groove and its soft outlines suggest a rather old age. The apparently different ages of these landslides on Phobos suggest that their formation occurred throughout the entire history of Phobos and were probably induced by seismic effects of close and distant cratering events. This also suggests that during the period of heavy bombardment, the formation of landslides was more frequent than in the current geologic epoch.

Fig. 15 shows hummocky terrain of the Stickney crater floor, interpreted as deposits of one or several landslides in comparison with landslide deposits on the floors of craters on the Moon and Iapetus.

It is seen in Fig. 15 that the hummocky terrain on the Stickney crater floor looks rather similar to the hummocky terrains on the floors of the lunar crater Giordano Bruno (e.g., Shkuratov et al., 2012) and the Iapetus crater Malun (e.g., Singer et al., 2012) and probably is a deposit of one or several landslides. The inner slopes of Stickney crater, especially on its northern and western sectors, are steep enough to be surfaces formed by sliding: 35–45° (Giese et al., 2005; Willner et al., 2014). So hummocky terrain on the crater floor is a good candidate for slumping and landslide deposits; such an interpretation has been considered in detail by Shingareva and Kuzmin (2001).

3. Color units seen in the vicinity of crater Stickney and their geological context

Color units on the surface of Phobos designated "red" and "blue" were first described by Murchie et al. (1991) based on analysis of the spectrophotometric data taken by the VSK and KRFM instruments of the Phobos 2 spacecraft. Their compositional significance and interpretations are described by Pieters et al. (2014). Here we consider the geological context of these units through the geological analysis of the HiRISE color image of Stickney crater and its vicinity on which these units are well seen (Thomas et al., 2011). Fig. 16 shows an oblique view of the crater Stickney that was described by Shingareva and Kuzmin (2001) as the site of a giant landslide.

Shingareva and Kuzmin (2001) suggested that part of the massive landslide moving down from the W-NW sector of the crater inner walls (1 in Fig. 16b) reached the crater floor, forming the hummocky surface texture deposit (2 in Fig. 16b). In their interpretation of the event the landslide body acquired sufficient momentum for the frontal part of the moving landslide mass to travel up the interior of the wall and onto the eastern rim of the crater (3 in Fig. 16b), and then moved several kilometers further, spreading out toward the sub-martian point. The surface morphology of the eastern crater rim is generally hummocky (although with numerous grooves), a point that they cited as agreeing with their suggestion that this was a part of the landslide. On the other hand, this same morphology also agrees with the interpretation of Thomas (1998), who suggested that this area was the product of an asymmetric ejecta deposit from Stickney crater.

It is seen in Fig. 16 that the northwestern and northern parts of the crater rim are red. The inner slopes beneath this part of the rim appear reddish; however, two small craters in the lower part of the reddish slope have blue ejecta suggesting that underlying the red material of the surface slope there is blue material. The red and reddish surface material is typical, for the most part, of the Stickney crater interior and the southern rim of the crater, thus composing an extended red unit.

The hummocky terrain of the crater floor is dark gray and slightly bluish. Within it there are observed several small craters with blue ejecta and two craters with red ejecta. This suggests that the floor material here may be a coarse mixture of both the red and blue units.

The eastern rim of crater is mostly blue, forming a distinct color unit. In this location a 700 m crater (4 in Fig. 16b) is observed, whose interior, eastern rim and area further to the east are red, while the area around the crater is blue, except that part to the east. This suggests that this crater excavated the red unit, underlying the blue unit. The absence of red material excavated by this crater on the west rim may be due to oblique impact producing asymmetric ejecta. The fan of red material extends from the eastern rim of this crater towards the east for about 1.2 km. This fan is on a slope inclined to the east (10–15°, Giese et al., 2005; Willner et al., 2014) of the external part of the Stickney rim and at least partly might represent a case of downslope movement by a creep mechanism. A pure case of oblique impact producing asymmetric ejecta, as proposed by Thomas (1998), can also not be excluded.

The presence of red material beneath the layer of blue material is also suggested by the observation of several craters ~100–300 m in diameter having red ejecta or red rims. One of these, about 100 m in diameter (5 in Fig. 16b) is surrounded by a relatively wide (200–500 m) red halo, interpreted as its ejecta. Red material is also seen along the rim crests of some grooves in this area. At the same time, two relatively large craters (700 m and 1 km in diameter) to the west of the red halo crater, and several relatively small craters to the west and to the east of the haloed crater, excavate blue material, suggesting that either (1) the blue ejecta of Stickney is thicker here than in the locality of the small red-ejecta craters described, or (2) the blue ejecta here is superposed on blue bedrock material.

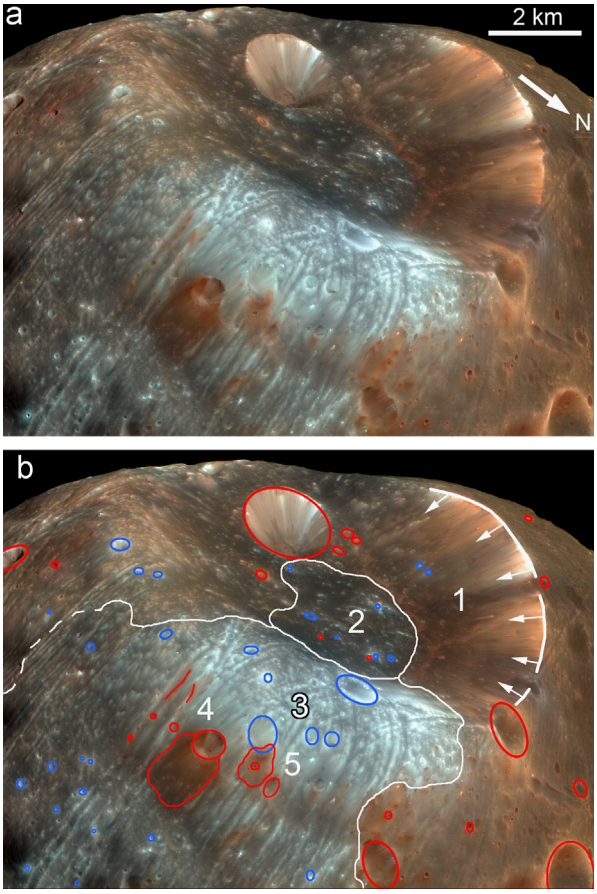

Fig. 16. (a) An oblique view of Stickney crater and its eastern rim. (b) Same view with the key geologic features marked. Craters excavating the red and blue materials are outlined with red and blue, correspondingly. Red lines designate the outcrops of reddish material along the rim crests of the grooves. White lines show boundaries of geologic units. Image HiRISE_PSP_007769_9010_IRB synthetized from the images taken in infrared (800–1000 nm), red (550–850 nm), and blue–green (400–600 nm) channels. (For interpretation of the references to color in this figure legend, the reader is referred to the web version of this article.)

A few craters in the western part of the Stickney crater interior, including the 2-km crater Limtoc, as well as two craters on the Stickney southern rim (100 m and 1 km in diameter), all within the red unit, have red rims or ejecta. But three craters on the very crest of the southern rim of Stickney crater have blue rims. The latter suggests the presence of blue material beneath the red material. In this case the red material may be ejecta from crater Limtoc covering the blue material of this part of Stickney ejecta.

The relationships observed in Fig. 16 in terms of the morphology and distribution of red and blue color units within Stickney crater and its vicinity, are summarized in the schematic illustrative diagram of Fig. 17.

We consider two different model cases for the structure of the target material and thus in the potential consequences of formation of Stickney crater and the small craters superposed on its eastern rim and northern inner slope. These cases are related to potential options for the origin of the red and blue units discussed.

Case 1. implies that Phobos material is basically blue, covered by the red relatively thin mantle formed either due to space weathering or to a supply of red material from an external source (interplanetary dust?) (a in case 1). Stickney crater penetrates

through the red mantle into the blue material and its ejecta all around the crater is a mixture of red and blue materials (b in case 1). The smaller crater superposed on the Stickney rim penetrates through the Stickney ejecta, the red mantle, and excavates the underlying blue material, so ejecta of this smaller crater is essentially blue (see the inset in the left part of case 1). Another smaller crater superposed on the inner slope of Stickney penetrates through the thin red-and-blue talus and excavates the blue material, so ejecta of this smaller crater is essentially blue (see the inset in the right part of case 1).

Case 2. implies that Phobos is primarily a heterogeneous object consisting of a mixture of blocks of red and blue materials of different sizes. In this case it is suggested that in this given area there was a block of blue material several kilometers across and more than 1–2 km thick, surrounded by red material (a in the case 2). Stickney crater is superposed on the area of the boundary between the blocks of the red and blue materials, so one part of its ejecta is blue while another part is essentially red (b in the case 2). The smaller crater superposed on the Stickney blue ejecta of its eastern rim penetrates through the ejecta and excavates the underlying red material, so the ejecta of this smaller crater is essentially red (see the inset in the left part of case 2). Another smaller crater superposed on the inner slope of Stickney penetrates through the thin red-and-blue talus and excavates the blue bedrock material, so its ejecta is essentially blue (see the inset in the right part of case 2).

Comparing the two model cases (Fig. 17) with observations (Fig. 16), we see that the E-SE segment of the Stickney rim is blue while the remaining part of the rim is red. This corresponds to model case 2. Several craters superposed on the blue eastern rim of Stickney crater show red ejecta. This also agrees with model case 2. Two craters superposed on the essentially red lower part of the northern inner slope of crater Stickney show blue ejecta. This agrees both with model cases 1 and 2. The comparisons of the model cases, considered together with these observations, show that model case 1 disagrees with observations in 2 of three tests, while model case 2 agrees with observation in 3 of three tests. We therefore interpret model case 2 to be closer to reality.

We believe that this model best explains the relations of the red and blue materials observed on the HiRISE image analyzed. An important implication of the model is that the red and blue materials form blocks, at least some relatively large, composing the body of Phobos; this generally agrees with earlier suggestions by Murchie et al. (1991). Crater ejecta and downslope material movement redeposit these materials, forming secondary and tertiary derivatives of these color material units and their mixtures. The illustrated scheme suggests that a mantle of blue material on the eastern rim of Stickney crater is the crater ejecta deposit (e.g., Thomas, 1998) but we cannot rule out the interpretation of Shingareva and Kuzmin (2001) that it is a tongue of a runout landslide.

4. Ejecta from Mars on Phobos

The proximity of Phobos to Mars and the great number of impact craters observed on the surface of this planet imply the possibility that some high-velocity part of ejecta from Martian craters may reach the surface of Phobos and become part of its regolith. Britt and the Gulliver Team (2003), in proposing the Gulliver mission designed to return samples from Deimos, more than three times further from Mars than Phobos, estimated that "Mars material may make up as much as 10% of Deimos's regolith". It is logical to expect that the Phobos regolith should also have an admixture of Mars material and it was discussed in a number of

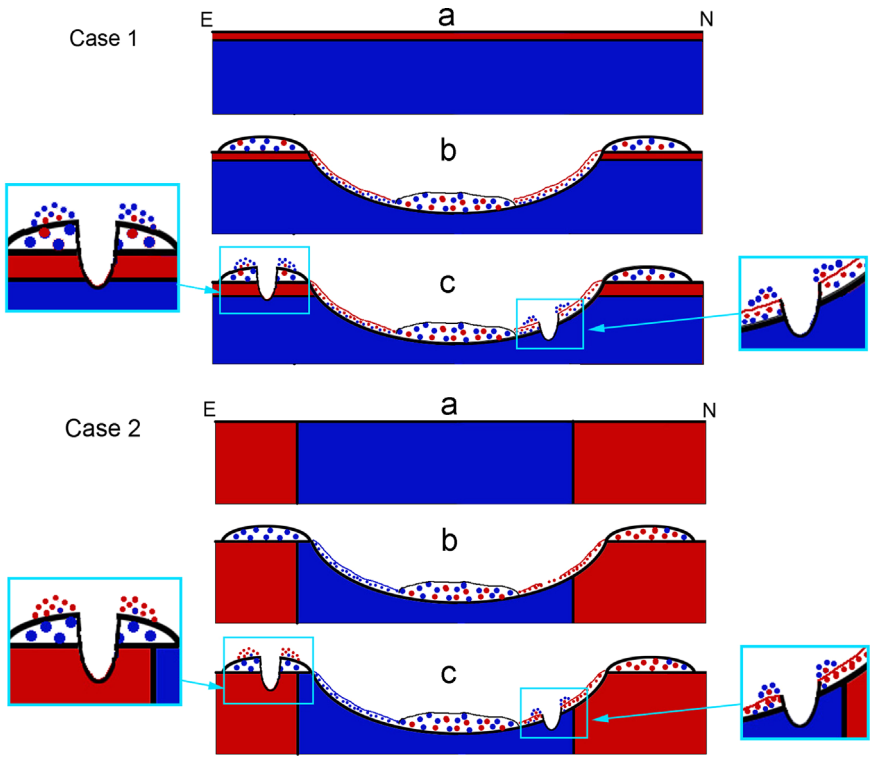

Fig. 17. Schematic illustrative diagram of a profile from the eastern rim of the crater Stickney towards the crater center and then to its northern rim. Rim structure and bedrock deformation has been omitted. The stages of formation of the observed morphology and distribution of the red and blue units are shown: (a) stage 1, (b) stage 2 and (c) stage 3 for two cases (see text). (For interpretation of the references to color in this figure legend, the reader is referred to the web version of this article.)

publications (e.g., Murray et al., 1994; Lee, 2009; Chappaz et al., 2012; Ramsley and Head, 2013a). Below we review this issue based on published literature, including the recent results of calculations by Ramsley and Head (2013b).

Ramsley and Head (2013a,b) used Keplerian orbits (elliptical and hyperbolic) for fragments ejected from Mars to assess the mode of arrival and impact of Mars ejecta on Phobos, the amount of Mars ejecta that might have been delivered to Phobos, the types of features that these impacts would produce, and the fate and current location of these ejecta on Phobos. They found that primary ejecta from Mars typically impacts Phobos at velocities of ~2–3 km/s. Due to the low escape velocity from Phobos of ~4–10 m/s, ~95–99% of the secondary ejecta from Phobos is inserted into temporary orbits around Mars and most Phobos ejecta fragments remain trapped in orbits around Mars for several days to several thousand years until they re–impact with Phobos and produce new generations of ejecta. Mars–orbiting Phobos ejecta fragments typically re–impact on opposite hemispheres of Phobos from their previous impact sites. Combining this with the typical conical dispersion pattern of impact ejecta, Ramsley and Head (2013b) found that two or three generations of re–impacts on Phobos on the alternating opposite hemispheres are sufficient to uniformly disperse Mars ejecta fragments globally across the geographic surface of Phobos.

Ramsley and Head (2013a) also predict a size sorting of regolith from these processes. While in orbit around Mars, particles of ejecta are perturbed by martian gravity and solar photon forces that combine to produce an increase in the orbital eccentricities; this preferentially alters the orbits of the smallest fragments. Dust fragments $< \sim 300$ μm are typically de–orbited to the atmosphere of Mars or to solar orbits within several years, whereas fragments $> \sim 300$ mm tend to remain in orbit until they re–impact with Phobos. The rapid removal of dust fragments $< \sim 300$ μm places a severe limit on their opportunities for a re–impact with Phobos and Ramsley and Head (2013a) predict a deficiency of dust grains $< \sim 300$ μm in the regolith of Phobos.

For the present day altitude of Phobos, Ramsley and Head (2013a) calculated that the flux from solar system projectiles that impact Phobos is ~200 times greater than the flux from primary Mars ejecta. Based on lunar regolith observations, the bulk concentration of solar system projectiles in the regolith of Phobos is likely to be ~3%, which suggests a bulk concentration of Mars ejecta fragments in the regolith of Phobos of ~150 ppm (3%/200). Compared with the Moon, the vicinity of Mars experiences a higher flux rate and lower average impact velocity from asteroidal projectiles (Ivanov, 2001). These differences combine to increase the abundance of Mars ejecta in the regolith of Phobos from ~150 ppm to ~250 ppm. Phobos has orbited at least farther from Mars during all but the most recent ~500 Ma; thus, through the majority of the early geological history of Phobos, ejecta plumes from Mars would have expanded to a much larger volume and would have diffused to substantially lower volumetric density at the point of intersection with Phobos. Ramsley and Head (2013a) suggest that their computed ~250 ppm bulk concentration of Mars ejecta in the present day may be found preferentially closer to the younger upper regolith of Phobos. At depth, Mars ejecta fragments are likely to be found in bulk concentrations that are 1 to 2 orders of magnitude less than near the surface of Phobos.

In summary, Ramsley and Head (2013a,b) predict that (1) the geographic distribution of Mars ejecta fragments in the regolith of Phobos is isotropic; (2) the bulk concentration of Mars ejecta fragments in the upper regolith of Phobos is ~250 ppm; (3) ejecta fragments from Mars are most densely concentrated in the upper half meter of the Phobos regolith; and 94) the regolith of Phobos is likely to be deficient in dust fragments < 300 μm.

5. Grooves

In addition to craters, grooves represent another type of feature inherent to the surface of Phobos, and their characteristics, distribution and origin are reviewed in detail in Murray and Heggie (2014). Here we consider only some of their main characteristics and briefly describe their potential morphologic analogs on other bodies of the solar system. Comparative consideration of the characteristics of Phobos grooves and their potential analogs may put constraints on the origin of grooves.

5.1. Some characteristics of the grooves

Phobos grooves are elongate, linear or almost-linear depressions typically 100–200 m wide and 10–30 m deep. Their lengths are typically a few kilometers but may reach about 20 km (Thomas et al., 1979). They vary in their appearance from chains of coalescing pits of approximately the same diameter to grooves with scalloped margins and to grooves with almost linear margins. Fig. 18 shows the morphologic varieties of grooves and the relations between grooves and large craters, Drunlo (D=4.2 km) and Clustril (D=3.4 km).

It is seen in the Fig. 18 that groves criss-cross rims of these craters and their inner slopes and the visibility of these relations is strongly dependent on illumination conditions. Some grooves show raised rims that distinguish them from normal graben (see below in the discussion of potential martian analogs). Grooves crossing crater rims typically show continuity with no gaps; some trails of bouncing boulders seen on lunar crater slopes show gaps, while others do not (see below in the discussion of potential lunar analogs).

The grooves on the surface of Phobos form crisscrossing systems of subparallel features - different “families” (Thomas et al. 1979). Different families (the number of families is at least 12), are considered by some authors to have formed in separate formational episodes (Murray et al., 2006; Murray and Iliffe, 2011). Fig. 19 shows typical example of the intersections of grooves.

It is seen in the Fig. 19 that at the intersections of grooves of different orientation, no prominent lateral offsets are seen, in contrast to what is often seen at the intersections of various tectonic features (compare below with martian graben).

Some families are spatially very extensive, covering areas with latitudinal or longitudinal extent larger than 90–120°. Fig. 20 shows a portion of one such north-south-trending family.

It is seen in Fig. 20 that the north–south trending grooves show approximately the same morphology along the entire area. This characteristic may be significant in discussing some mechanisms of groove formation (see below).

5.2. Potential morphologic analogs on other bodies of the solar system

Some linear features on different bodies of the solar system resemble the grooves on Phobos to a greater or lesser degree. Among these are tracks of rolling and bouncing boulders on the slopes of lunar landforms (e.g., Head and Wilson, 2011; Duxbury et al., 2011), pit chains and shallow troughs on Eros (e.g., Buczkowski et al., 2008, 2009), pit chains and troughs on Lutetia (e.g., Thomas and Prockter, 2010; Thomas et al., 2012), and troughs on Vesta (e.g., Buczkowski et al., 2012). Comparisons with systems of linear faults on Mars (e.g., Wilson and Head, 2002) may also be useful. Below we show and briefly describe these features.

Fig. 21 shows tracks produced by rolling and bouncing boulders on the slopes of lunar craters seen in LROC NAC images.

Fig. 21 shows that the tracks of rolling and bouncing boulders on the Moon look very similar to the pit chains displayed by a variety of

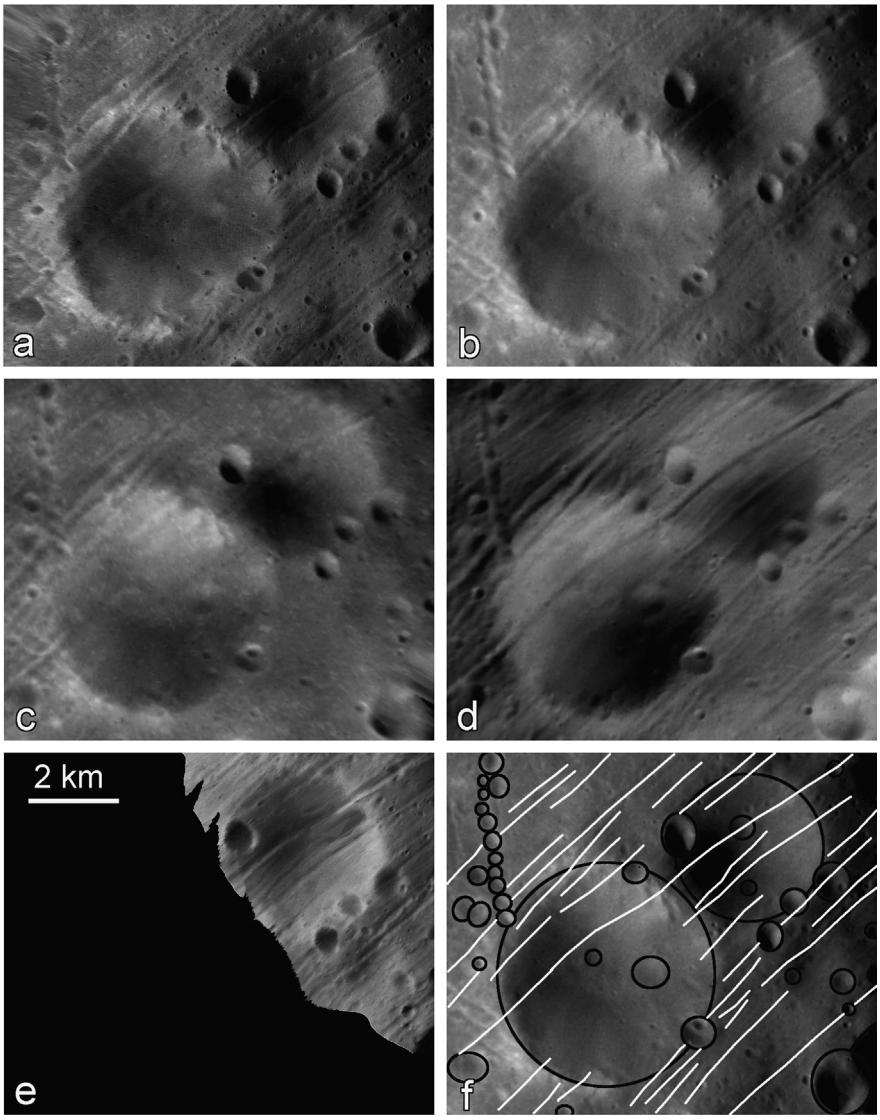

Fig. 18. HRSC images of Drunlo crater (lower left) and Clustril crater (upper right). Shown are portions of images taken on orbits 0756 (image a), 2780 (b,f), 2813 (c), 3310 (d) and 5851 (e). All these images are reprojected for central longitude 31°W.

Phobos grooves. Two important observations are (1) boulders that produced the tracks are often seen at the ends of the tracks; (2) Fig. 21d shows that after crossing the positive landform (in this case, the crater rim) a boulder makes a large bounce and the interval between two markings here (20 m) is noticeably larger than in other places along this track (2–5 m). It is seen in the image that the inner slope steepness in this crater is close to the Sun elevation at the moment of imaging (~35°, http://wms.lroc.asu.edu/lroc/search). Simple calculations show that the velocity of the boulder along this track was ~7 m/s, that, in the case of Phobos, would result in a 4–5 km long flight and thus gap in the track.

Fig. 22 shows chains of coalescing pits and shallow troughs on the surface of asteroid Eros (34 km × 11 km × 11 km), seen in the NEAR MSI images.

It is seen in Fig. 22 that the pit chains and shallow troughs look rather similar to Phobos grooves and are approximately the same sizes. Some, like grooves of Phobos, have elevated rims (arrows in Fig. 22a). Buczkowski et al. (2008, 2009) describe different types of lineaments, including pit chains, groves, and flat-floored troughs on Eros. Many of them are radial to large craters or circumferential to them. But many have no obvious relationship to impact craters. In general, lineaments of Eros are considered as the surface expression of faults/fractures accumulated during the impacting/collisional history of this body (e.g., Thomas and Prockter, 2010). It is important to mention that Eros is rather close to Phobos in size, but different from Phobos in having no large body nearby.

Fig. 23 shows chains of coalescing pits and shallow troughs on the surface of asteroid Lutetia (121 km × 101 km × 75 km), which look rather similar to grooves of Phobos.

Pit chains and shallow troughs of one of the areas of the Lutetia surface are seen in Fig. 23. They are wider than grooves on Phobos (400–800 m versus 100–200 m) but relatively short (5–10 km). One set of such lineaments was traced for about 80 km (Thomas et al., 2012). Some pit chains have elevated external rims (see Fig. 26 in Thomas et al., 2012). The lineaments crisscross each other but not in such an obvious way as do the grooves of Phobos (see, for example, our Fig. 19). They do not seem to form as dense a network as grooves on Phobos do. But this observation may be due to the lower resolution of available images of Lutetia compared to the images of Phobos. Lineaments of Lutetia do not show any obvious radial relationship to any impact crater, but nevertheless they are interpreted to be the result of impact-induced seismic activity (Thomas et al., 2012). Lutetia is significantly larger than Phobos but still in the part of the asteroid domain for which

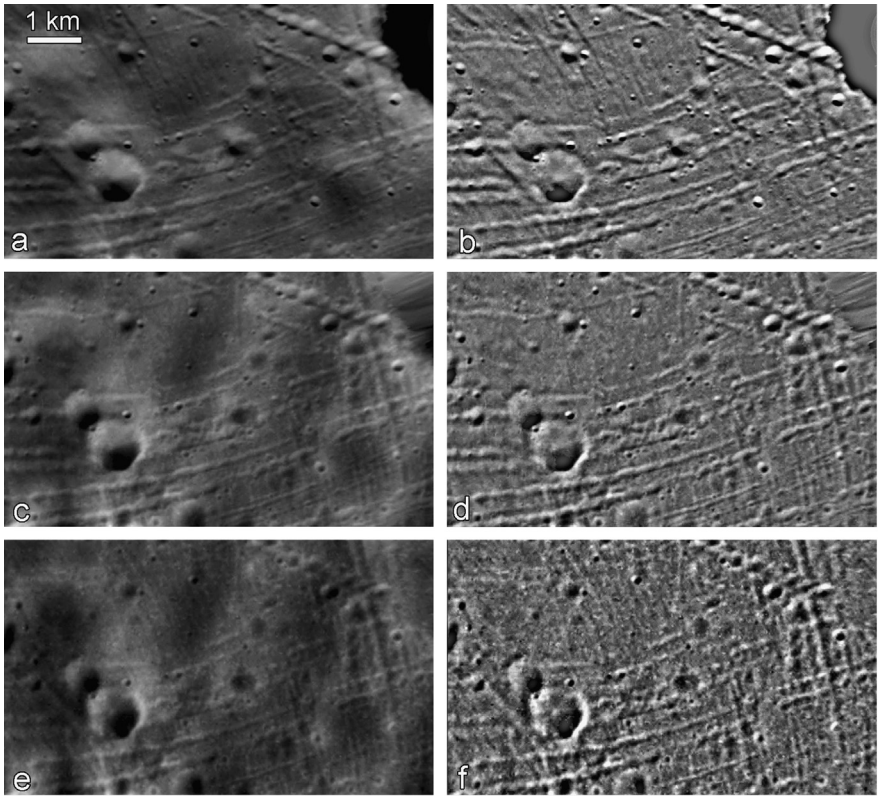

Fig. 19. Groove intersections SW of Drunlo crater. Portions of images taken on orbits 6906 (a,b), 4847 (c,d), and 2813 (e,f), reprojected for central longitude 102°W; left, original images; right, stretched to increase contrast.

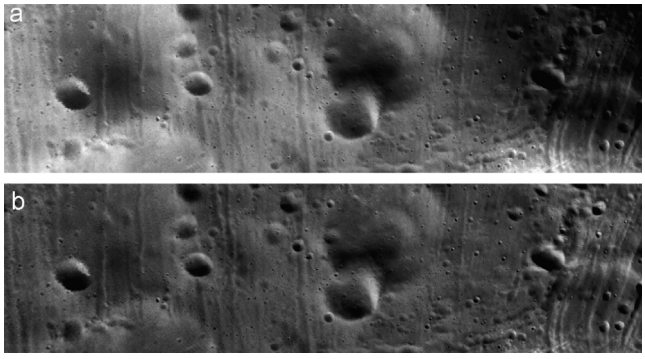

Fig. 20. Morphology of grooves across a large angular distance. Portion of image taken on orbit 0756 (central longitude 31°W) (a and b show different stretches of the image). Drunlo and Clustril craters are in the left part of the image, Reldresal crater is close to the image center. The image long axis is oriented approximately from west (left) to east (right) and covers the longitude range from about 0 to 130°W.

endogenic tectonics is not expected (e.g., Thomas and Prockter, 2010). In contrast to Phobos, Lutetia (like Eros) does not have a large body nearby.

Fig. 24 shows troughs on asteroid Vesta (578 km × 560 km × 459 km) that resemble grooves on Phobos in their appearance.

The troughs are linear features, often with scalloped rims. They range from several to ~20 km wide and are up to hundreds of kilometers long. The troughs trend generally in an east–west direction, forming a near-equatorial cluster from ~45° W to the central meridian and then to ~135° E. They are considered to be graben (Buzckowski et al., 2012). It is important to note that Vesta is significantly larger than Phobos. It underwent magmatic differentiation (Keil, 2002 and references therein), so endogenic tectonics might be expected at this body. Instead, the origin of the graben is interpreted to be related to the impact events that formed the Rheasilvia and Veneneia basins at the south pole of Vesta (Buzckowski et al., 2012). As in the case of Eros and Lutetia, and contrary to the case of Phobos, Vesta does not have a large body nearby.

Fig. 25 shows two kinds of faults of Mars relevant to our discussion. These faults are different in morphology from grooves on Phobos, but their characteristics may be useful in consideration of the origin of grooves on Phobos.

Fig. 25a shows intersecting faults in Elysium Planitia, Mars. This type of intersections is considered to be a classic one, with the lateral offset of the younger faults at the intersection with the older ones (Lachenbruch, 1962; Kulander et al., 1979). In this given case at least three generations of faults can be distinguished (1) two older faults trending from W to E, 2) three younger faults trending generally N–S, and one, the youngest fault, trending SW–NE.

Fig. 25b shows intersecting graben near Alba Patera. These graben are flat-floor troughs 0.5–2 km wide and tens of kilometers long, with steep inner slopes and no topographic elevations at their edges. Two sets of graben are seen here with obvious age relations: the older trending N–S and the younger trending SW–NE. No lateral offset at the intersections of the younger graben with the older ones are seen. It is not clear why the classic rule described by Lachenbruch (1962) and Kulander et al. (1979) does not work here but this example shows that the absence of lateral offsets may be the case. One possible reason is that these graben are formed due to wedging and opening from below by magmatic dikes (Wilson and Head, 2002).

5.3. Notes on the origin of Phobos grooves

The origin of Phobos grooves has been under debate since their discovery in 1976–77. There is a group of hypotheses considering grooves of Phobos as fractures/faults which formed by (1) Stickney

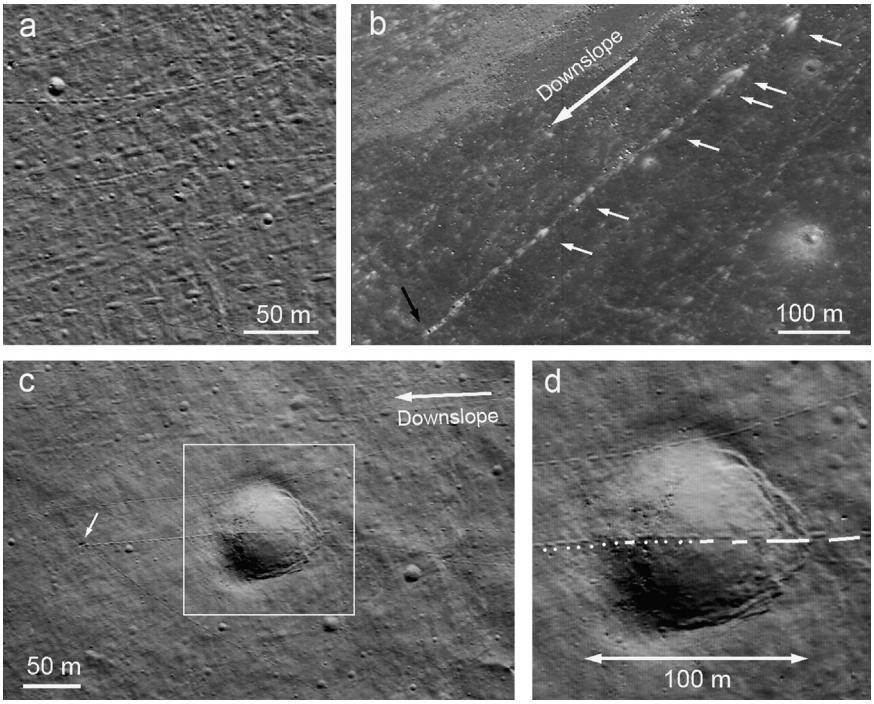

Fig. 21. Tracks of rolling and bouncing boulders on slopes of lunar craters. Framelets a, c and d show tracks in the lower part of the eastern inner slope of a 15-km crater at 52°N, 191°E; white arrow on framelet c shows the boulder (d=2–3 m) which produced the track shown in framelets c and d; thick white lines and dots in framelet d show gaps in between markings produced by the bouncing boulder. LROC NAC image M107985155LE. Framelet b shows a track produced by a ~5-m boulder (black arrow) on the northeastern segment of the inner slope of a 30-km crater at 37°N, 185°E, image M110383422RE.

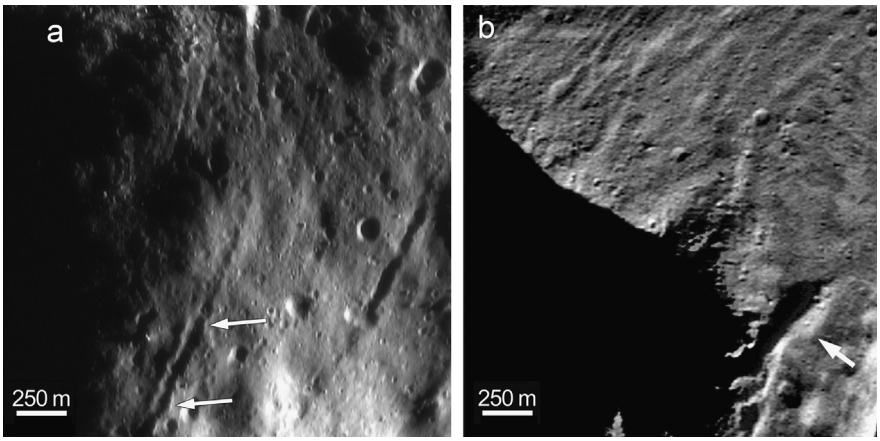

Fig. 22. Chains of coalescing pits and shallow troughs on the surface of Eros.The NEAR Multi-Spectral Imager images 135344864 (a) and 127521108 (b). In the lower right of framelet b, Rahe Dorsum ridge is seen (arrow).

(and other crater) impacts (Thomas et al., 1978), (2) by tidal forces (Soter and Harris, 1977; Weidenschilling 1979; Dobrovolskis, 1982), and (3) by drag forces when Phobos was captured by Mars (Thomas et al. 1979; Pollack and Burns, 1977). Other authors considered the grooves of Phobos as chains of secondary impact craters or ejecta from Stickney (Veverka and Duxbury, 1977; Head and Cintala, 1979; Davis et al. 1980). A variation on the latter view is the suggestion that grooves on Phobos were formed by rolling blocks, some of which are ejecta from Stickney crater (Head and Wilson, 2011; Duxbury et al., 2011). Another hypothesis suggests that grooves on Phobos are chains of secondary impact craters caused by large primary impacts on Mars (Murray et al. 1994, 2006). Below, based on the descriptions of Phobos grooves given above and their potential analogs on other bodies of the Solar system, we briefly consider the suggestions that they are (1) fractures/faults, (2) tracks of rolling and bouncing boulders, and (3) chains of craters formed by ejecta from large impact craters of Mars. An extensive discussion on the origin of Phobos grooves can be found in Murray and Heggie. (2014).

5.3.1. *Grooves as fractures/faults*

We do not discuss here what might cause the fractures/faults if they are fractures/faults. All three factors mentioned above – impact seismicity, tidal forces and the capture drug forces – could work separately or together. The suggestion that the grooves are fractures/faults agrees with their linear morphology and cross-cutting relations with relatively old craters. It is indirectly supported by observations of linear features to varying degrees similar to Phobos grooves on other small bodies, Eros, Lutetia, Vesta, for which other factors of formation mentioned are not considered possible. Two characteristics of Phobos grooves, namely, the elevated rims

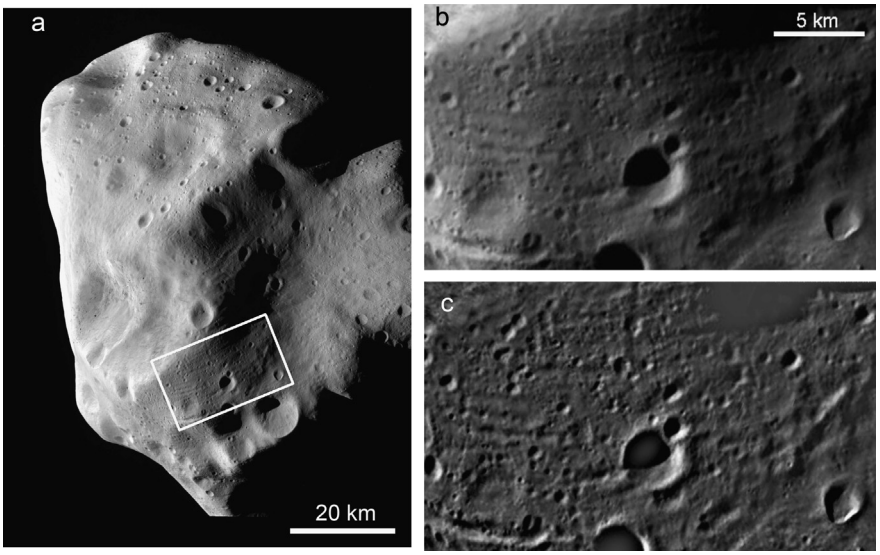

Fig. 23. Asteroid Lutetia. (a) General view, white rectangle outlines area shown in framelets b and c, (b) area with grooves and pit chains, (c) the same image processed by high-pass filtering. Images of Osiris camera, Rosetta mission. Source: http://www.esa.int/images/4-c_closest_approach.0.jpg.

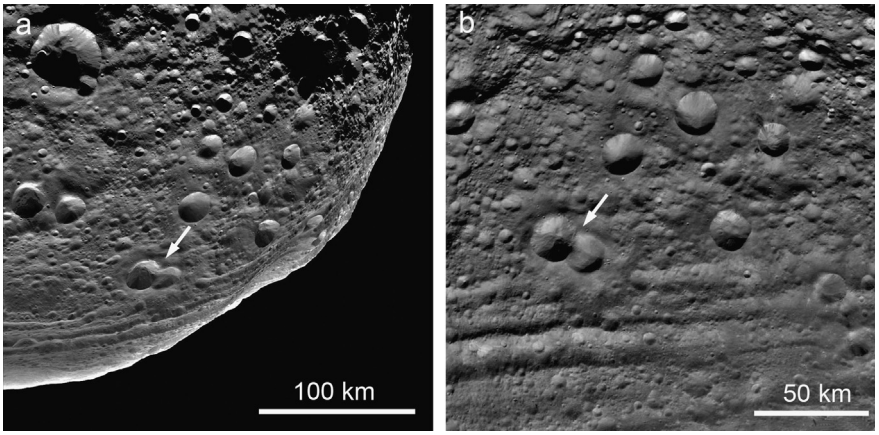

Fig. 24. Troughs in the equatorial region of Vesta. Arrow in framelets a and b show the same pair of craters. Framing Camera images11f2_355888320 and 8f2_365889442, correspondingly.

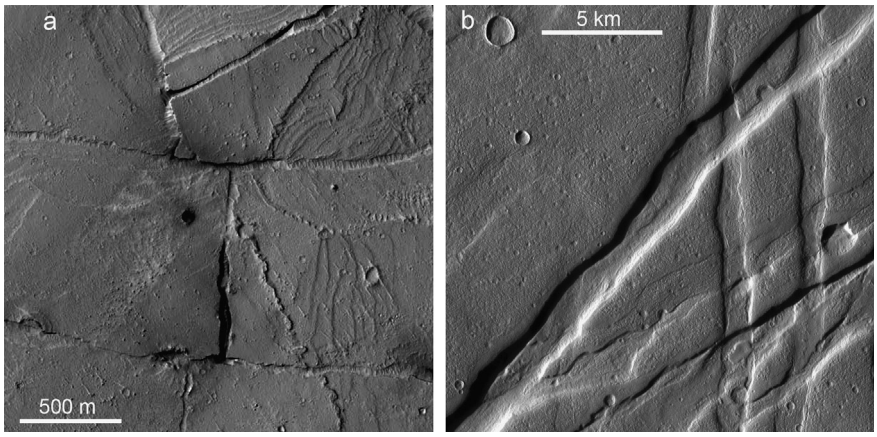

Fig. 25. (a) Intersecting faults with lateral offsets in Elysium Planitia; HiRISE image PSP-010348-1870. (b) Intersecting graben near Alba Patera. No lateral offset at the intersections of the younger (diagonal) faults with the older ones (horizontal) is seen. THEMIS image V20111005, north is to the right.

displayed by many of them, and the absence of lateral offsets at the intersections of grooves of different families and probably different age, could be considered as evidence against the fracture/fault suggestion. But the elevated rims are seen in the case of lineaments of Eros and Lutetia described above (Fig. 22 and Fig. 26 in Thomas et al., 2012) and faults (graben) on Mars also show no lateral offsets

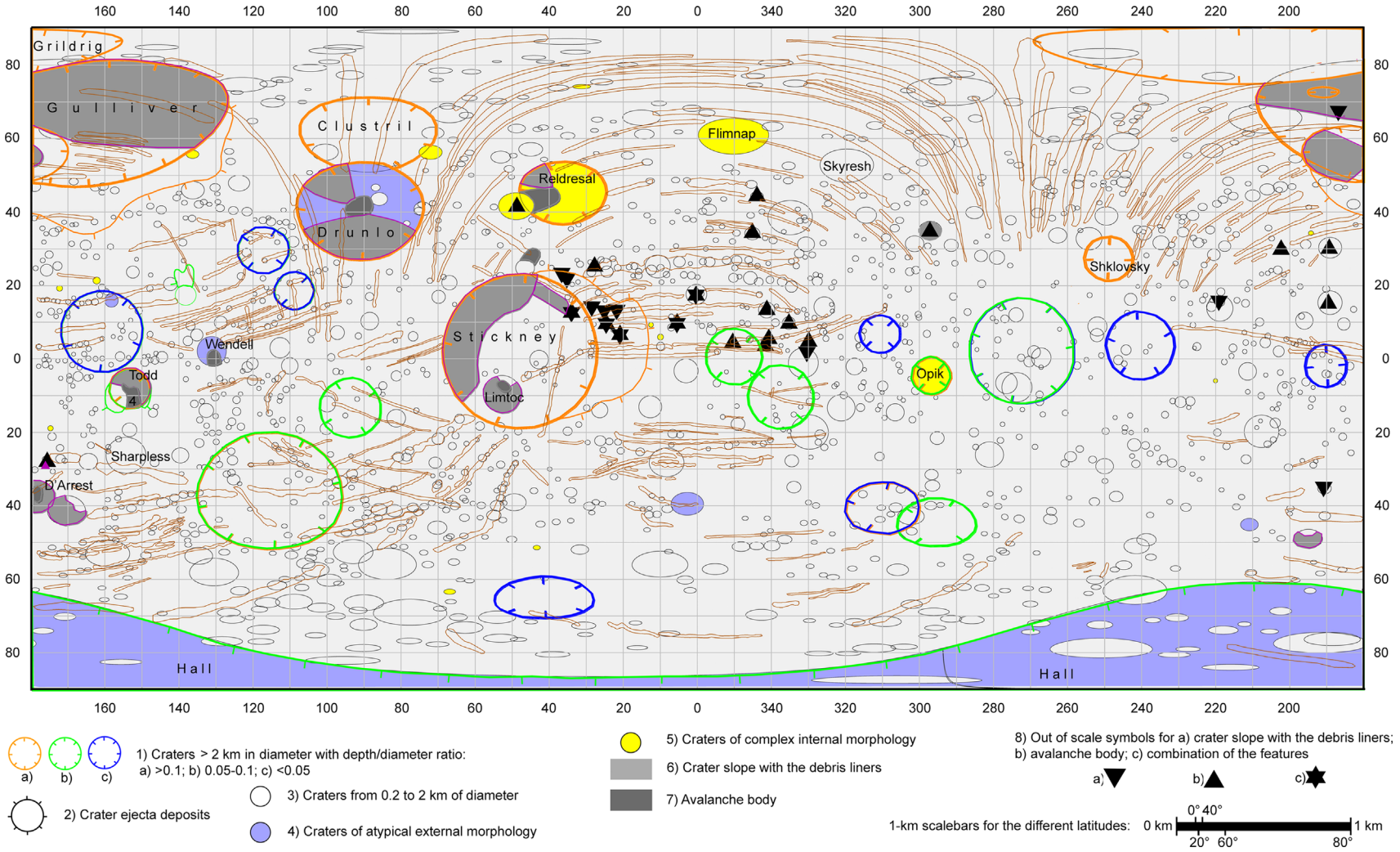

Fig. 26. Geomorphic map of Phobos. Simple cylindrical projection. Scale bars at different latitudes are shown.

(Fig. 25b). Also if Phobos grooves are significantly wider than the faults underlying them, then this widening might mask any small-scale offsets.

5.3.2. Grooves as tracks of rolling and bouncing boulders

Detailed consideration of the potential mechanism of formation of Phobos grooves associated with Stickney crater as tracks of rolling and bouncing boulders ejected from this crater is given in Wilson and Head (2014). As these authors show, this suggestion agrees with the morphology and structure of the grooves, estimates of the soil properties, the boulder size, strength and geometry, the exit velocity, the friction factor, and the variable gravity on Phobos. Two difficulties with this hypothesis are absence of boulders at the end of the grooves and the absence of gaps behind the positive topography, such as the rims of large prominent craters, two features often observed in the case of the boulder tracks on the slopes of lunar landforms (Fig. 21). The lunar examples (Fig. 21) are very young, however, and on Phobos boulder degradation and destruction since groove formation could readily destroy such evidence. Further, groove continuity is a function of velocity, and Wilson and Head (in preparation) have shown that velocities for blocks ejected from Stickney are such that continuous grooves can readily form across traversed crater interiors and rims.

5.3.3. Grooves as chains of craters formed by ejecta from impact craters on Mars

Detailed consideration of the formation of Phobos grooves by this mechanism is given in several publications by J. Murray and his coauthors (e.g., Murray et al., 1994, 2006; Murray and Iliffe (2011). Recently, Ramsley and Head (2013a) tested this hypothesis by plotting precise Keplerian orbits for ejecta from Mars. They found, in particular, that to emplace families of parallel grooves as observed, and to reach the maximum geographic extent on Phobos, grid patterns of ejecta fragments must be produced with nearly identical diameters and must launch with virtually zero rates of dispersion. The irregular topography and small-body radius of Phobos should clearly disrupt groove family linearity and parallelism due to the preponderance of oblique incident angle impacts. However, the vast majority of groove families and individual grooves appear to completely avoid the effects of the morphology of Phobos. Also, the hypothesis of Murray et al. (1994) seems to contradict the observation that the groove morphology does not change significantly within the families which occupy areas as large as 90 to 130° of angular (longitude) size (Fig. 18). Another problem with this interpretation of Phobos grooves is the fact that the asteroids discussed above display groove-like features but do not have a nearby "Mars" for secondary crater-forming material to originate. Finally, the flux of Mars ejecta that would be required to produce the groove pits is insufficient by many orders of magnitude (Ramsley and Head, 2013a,b). More work is certainly needed to resolve disagreement among the different hypotheses for the origin of grooves on Phobos.

6. Summary and conclusions

The above descriptions and considerations may be summarized in the geomorphic map of Phobos (Fig. 26) and in the following text.

The major landforms on Phobos surface are (1) craters, mostly impact, the analysis of which provides information on the cratering process, target materials, downslope material movement, brightness and color units of Phobos materials, and (2) grooves, whose morphological characteristics are reasonably well described, but their origin is debated.

6.1. Craters

Phobos is an irregularly shaped body, 26 km × 22.8 km × 18.2 km with ~1300 craters ≥200 m in diameter, ~70 craters ≥1 km, ~30 craters ≥2 km identified on its surface; the largest crater on Phobos, Stickney, is about 8 km in diameter. Most craters are undoubtedly of impact origin although some small craters may be pits formed by drainage of regolith into subsurface fractures. The presence of the observed impact crater population implies that the upper hundreds of meters to a few kilometers of Phobos should be heavily fractured.

Using the Phobos surface DTM, the 24 craters larger than 2 km in diameter were subdivided into three morphologic classes on the basis of their prominence with the following values of d/D ratios and maximum steepness of their inner slopes: >0.1 and >20°, 9 craters; 0.05–0.1 and 10–20°, 7 craters; and <0.05 and <10°, 8 craters. This subpopulation of Phobos craters has a considerably larger number of gentle-walled craters compared to lunar highland craters, and this may be due to several potential factors including the very small surface gravity of Phobos.

Most craters on Phobos are bowl-shaped, but some interiors contain complex morphology, for example, concentric, flat-bottomed and craters with central-mounds. The size of these craters displaying complex morphology is indicative of layering in the target material: a layer of regolith covering bedrock as well as layers within the regolith. The thickness of the regolith is estimated to vary from 5 to 100 m. Layering within the regolith is apparently not continuous, but lens-like. The presence of layering within the regolith is also suggested by observations of crater ejecta sometimes having various apparent brightnesses.

The regolith of Phobos, as on other atmosphereless bodies, resulted from accumulation of impact crater ejecta. But in the case of Phobos it was accumulated both by direct ejecta deposition and also through the return of the high-velocity fraction that escaped to near-Mars space during impact events. An important peculiarity of the Phobos regolith is the suggested deficiency in the <300 μm size fraction and presence of the Martian material with concentrations ~250 ppm in the upper 0.5 m and by 1-2 orders of magnitude lower at larger depth.

In some areas of Phobos, blocks of solid rock larger than a few meters in diameter are seen. Their distribution on the Phobos surface is not reliably known because of insufficient resolution of the available images. One of the known localities of rock blocks is near Stickney crater but because the age of Stickney is much larger that the survival time of blocks (estimated through analogies with survival time of lunar rocks; Basilevsky et al., 2013), the relation of these blocks and Stickney may not be primary. Alternatively, the age of Stickney derived from superposed impact crater size-frequency distribution may be in error.

Crater inner slopes and sometimes outer slopes of crater rims are localities of downslope material movement, as shown by the presence of downslope-trending albedo streaks and hundreds of meters to a kilometer size mounds on the floors and slopes of the craters. The albedo streaks are interpreted to be traces of geologically recent talus and avalanches. The mounds are considered to be landslide bodies. Different degrees of morphologic sharpness of the mounds suggest that they differ in age.

6.2. Color units

The distribution and mutual relations of "red" and "blue" units characteristic of Phobos surface material have been studied through geologic analysis of the MRO HiRISE color images of Stickney crater and its surroundings. Under analysis were observations of relatively small (hundreds of meters in diameter) craters having red and or blue ejecta and their positions on different parts of Stickney crater. As a result of this analysis it was concluded that

the red and blue "primary" materials may form relatively large blocks composing the body of Phobos, generally in agreement with earlier conclusions of Murchie et al. (1991). Crater ejecta and downslope material movement redeposit these materials, forming secondary and tertiary derivatives of these color material units and their mixtures. This conclusion, however, should be confirmed by observations in other areas of Phobos.

6.3. Grooves

These are typically 100–200 m wide and several kilometers long lineaments represented by chains of coalescing pits of approximately the same diameter, grooves with scalloped margins and grooves with almost linear margins. Grooves form several intersecting systems (families) of features with approximately the same orientation within each given family. Grooves often crisscross relatively large craters, including the crater rims, showing continuity with no gaps. This differs from some trails of bouncing boulders seen on the slopes of lunar landforms. Groove systems often intersect each other showing no lateral offsets at intersections. At least one of the groove families extends along a longitude for about 130°, an observation that should have implications for the formation mechanism of the groves.

Features similar to Phobos grooves are seen on other small bodies: Eros, Lutetia and Vesta. In morphology and size, grooves on Eros most resemble grooves on Phobos. Grooves on Lutetia are morphologically close to those of Phobos, but are significantly wider and relatively short. Grooves of Vesta are even larger, very continuous, and form a latitudinal belt in the equatorial part of Vesta.

Based on the above descriptions and consideration of three different mechanisms of Phobos groove formation, we conclude that (1) Grooves as fractures/faults: this mechanism agrees with the groove morphologies and relations with craters, although the elevated rims of some grooves and absence of lateral offsets at the intersections of grooves of different age is not consistent; the very consistent groove orientations within families along rather large distances is surprising if grooves are faults deforming coarsely brecciated blocky material beneath the regolith. (2) Grooves as tracks of rolling and bouncing boulders: this mechanism agrees with the groove morphologies, similar features on the Moon, and, if applied to the grooves associated with Stickney crater, with some groove orientations; the absence of boulders associated with grooves terminations and the lack of gaps where grooves cross positive topography have been cited as weaknesses. (3) Grooves as chains of craters formed by ejecta from impact craters of Mars: This third mechanism by (Murray et al. (1994, 2006); Murray and Iliffe (2011) makes predictions and interpretations of the groove morphologies and spatial patterns, but recent quantitative analysis of the trajectories and sizes of hypothetical martian crater ejecta blocks considered as forming grooves on Phobos, showed serious inconsistencies between the predicted and observed characteristics of the grooves (Ramsley and Head, 2013b). In addition, the presence of Phobos groove analogs on the bodies with no nearby "Mars" casts further doubt on this mechanism.

In conclusion, analysis of images and other information on Phobos shows that the surface of this body is dominated by two major geologic processes. The leading role belongs to impact cratering with associated target destruction, ejection and subsequent deposition, partly with a temporary stay in near-martian space. Shaking by impacts and stirring by day-night temperature changes cause surface granulated material to move down along-slope, directed by very low but nevertheless efficient surface gravity. Mechanism(s) of groove formation require additional studies.

In order to improve our understanding of the geological processes on Phobos and especially for understanding the origin of Phobos as a body, a sample return mission is crucially important. In addition to collecting material from Phobos itself, the returned sample is also likely to contain pieces of materials from Mars.

7. Some goals and objectives for future exploration on the basis of this research

1) *Grooves*: What is the origin of the grooves of Phobos? Are all grooves of the same genesis or are there multiple factors involved? Are they related to the low density of Phobos?
2) *Low Density of Phobos*: What factors are responsible for this? Is there water ice in the interior of Phobos or is the low density due to pore space?
3) *Age of Stickney*: What is the age of Stickney and how does this compare to the impact crater size-frequency distribution age?
4) *Regolith Formation*: How thick (and variable) is the regolith and how does the unusual gravitational environment of Phobos influence regolith formation processes?
5) *Boulders*: What is the origin of the boulders and boulder fields on Phobos? Do we understand their global distribution with available image data?
6) *Color Units*: What accounts for the distinctive color units on the surface of Phobos? Are they related to vertical or lateral heterogeneity?
7) *Zone of Exclusion*: What is the explanation for the zone where there appear to be no grooves?
8) *Composition*: What is the mineralogical makeup and petrological nature and diversity of Phobos.
9) *Mars Samples*: What is the abundance of ejecta from Mars in the soil and what is its mode of occurrence?
10) *Origin of Phobos*: What is the origin of Phobos and how does this compare to the origin of Deimos?

Acknowledgments

We would like to acknowledge P. Neivert, M. Waehliscjh, A. Kokhanov, I. Karachevtseva, M. Ivanov, M. Kreslavsky, P. Stook, and I. Antonenko for the help in working on this project. Part of the work of A.T. Basilevsky and C.A. Lorenz was supported by the joint grant of the Helmholtz Foundation and Russian Foundation of Basic Research (RFBR No 11-05-91323). Work by James W. Head and Kenneth R. Ramsley was funded by JPL Grant 1237163, for participation of JWH in the High Resolution Stereo Camera Team on the Mars Express Mission, which is gratefully acknowledged. Work of A.E. Zubarev was supported by Megagrant (No 11. G34.31.0021). This research was partly supported through NASA Solar System Exploration Research Virtual Institute (SSERVI) cooperative agreement at Brown University, which is gratefully acknowledged.

References

Andert, T.P., Patzold, M., Hausler, B., 2008. Precise mass determination of the Mars moon Phobos from Mars express close flybys. AGU Fall Meeting Abstr., A1431.
Archinal B.A., A'Hearn M.F., Bowell E. and 14 coauthors, 2011. Report of the IAU Working Group on cartographic coordinates and rotational elements: 2009. Celest. Mech. Dyn. Astron. 109, 101-135.
Basilevsky A.T..,1976. On the evolution rate of small lunar craters. In: Proceedings of the 7th Lunar Science Conference, pp. 1005–1020.
Basilevsky, A.T., Head, J.W., Hoerz, F., 2013. Rock boulders survival time on the surface of the Moon. Planet. Space Sci. 89, 118–126.
Basilevsky, A.T., Ivanov, B.A., Florensky, C.P., Yakovlev, O.I., Feldman, V.I., Granovsky, L.B., 1983. Impact craters on the Moon and the Planets. Nauka Press, Moscow p. 200 (p.(in Russian). See also technical translation in NASA Tech. Memo. TM-77667).
Basilevsky, A.T., Kreslavsky, M.A., Karachevtseva, I.P., Gusakova, E.N., 2014. Morphometry of small impact craters in the Lunokhod-1and Lunokhod-2 study areas. Planet. Space Sci. 92, 77–87.

Bibring, J.-P., Combes, M., Langevin, Y., 1989. 14 coauthors, 1989. Results of the ISN experiment. Nature 341, 591–593.
Britt D.T. and the Gulliver Team., 2003. The Gulliver mission: sample return from the Martian moon Deimos. LPSC-34, abstract #1841.
Buczkowski, D.L., Barnouin-Jha, O.S., Prockter, L.M., 2008. 433 Eros lineaments: global mapping and analysis. Icarus 193, 39–52.
Buczkowski, D.L., Barnouin-Jha, O.S., Wyrick, D., Prockter, L.M., 2009. Further analyses of the 433 Eros global lineament map (LPSC-40, abs. #1187).
Buczkowski, D.L., Wyrick, D.Y., Iyer, K.A., 2012. 17 coauthors, 2012. Large-scale troughs on Vesta: a signature of planetary tectonics. Geophys. Res. Lett. 39, L18205, http://dx.doi.org/10.1029/2012GL052959.
Carr, M.H., Crumpler, L.S., Cutts, J.A., Greeley, R., Guest, J.E., Masursky, H., 1977. Martian impact craters and emplacement of ejecta by surface flow. J. Geophys. Res. 82, 4055–4065.
Carrig, M., 1970. Experiments on the angles of repose of granular materials. Sedimentology 14, 147–158.
Chappaz, L., Melosh, H.J., Vaquero, M., Howell, K.C., 2012. Transfer of impact ejecta fragments material from the surface of Mars to Phobos and Deimos. AAS/AIAA Space Flight Mech. Meet. 12-212, 1–20.
Davis, D.R., Weidenschilling, S.J., Chapman, C.R., Greenberg, R., 1980. Dynamical studies of Phobos and Deimos: groove origin and ejecta dynamics. Rep. Planet. Geol. Progr. 1979–1980, 14–15.
Davis, D.R., Housen, K.R., Greenberg, R., 1981. The Unusual dynamical environment of Phobos and Deimos. Icarus 47, 220–233.
Dobrovolskis, A.R., 1982. Internal stresses in Phobos and other triaxial bodies. Icarus 52, 136–148.
Duxbury, T.C., 1974. Phobos: control network and analysis. Icarus 23, 290–299.
Duxbury, T., Robinson, M., Van Der, B.Ogert, C., Thomas, P.C., Neukum, G., Hiesinger, H., 2011. Phobos grooves: a lunar analogy. In : Proceedings of the 2nd Moscow Solar System Symposium. Absract 2MS3-MM-03.
Duxbury, T.C., Veverka, J., 1977. Viking imaging of Phobos and Deimos: an overview of the primary mission. J. Geophys. Res. 82, 4203–42111.
El-Baz, F., 1972. King crater and its environs. In: Apollo 16 Preliminary Science Report. NASA-SP-315, vol. 29–62, pp. 29–70.
Fanale, F.P., Salvail, J.R., 1990. Evolution of the water regime of Phobos. Icarus 88, 380–395.
Florensky, K.P., Basilevsky, A.T., Bobina, N.N., et al., 1976. Processes of reworking of surface of the Moon in Le Monier area based on results detailed studies by Lunokhod 2, Tectonics and Structural Geology. Planetology. Nauka Press, Moscow, pp. 205–234.
Florensky, K.P., Basilevsky, A.T., Gurshtein, A.A., et al., 1972a. On the problem of surface structure of lunar Maria, Modern Concepts about the Moon. Nauka Press, Moscow, pp. 21–45.
Florensky, K.P., Basilevsky, A.T., Gurshtein, A.A., et al., 1972b. Geomorphological Analysis of the Area of Mare Imbrium Explored by the Automatic Roving Vehicle Lunokhod 1. Space Research XII. Akademie-Verlag, Berlin, pp. 107–121.
Florensky, K.P., Basilevsky, A.T., Pronin, A.A., Popova, Z.V., 1971. Preliminary results of geomorphologic stydies of panoramas, Movable Laboratory on the Moon—Lunokhod 1. Nauka Press, Moscow, pp. 96–115.
Florensky, K.P., Basilevsky, A.T., Zezin, R.B., Polosukhin, V.V., Popova, Z.V., 1978. Geologic-morphologic studies of lunar surface. In: Movable Laboratory on the Moon—Lunokhod 1. V. 2. Nauka Press, Moscow, pp. 102–135.
Giese, B., Oberst, J., Scholten, F., Hoffmann, H., Spiegel, M., Neukum, G., 2005. the HRSC Co-Investigator Team, 2005. Ein hochauflo sendes digitales Oberflächen-modell des Marsmondes Phobos. Photogramm. Fernerkund. Geoinf. 5, 435–440.
Hawke, B.R., Blewett, D.T., Lucey, P.G., Smith, G.A., Bell, J.F., Campbell, B.A., Robinson, M.S., 2004. The origin of lunar crater rays. Icarus 170 (Suppl 1), S1–S16.
Head, J.W., Cintala, M.J., 1979. Grooves on Phobos: evidence for possible secondary cratering origin. Rep. Planet. Geol. Prog. 1978–1979, 19–21.
Head, J.W., Wilson, L., 2011. Origin of grooves on Phobos and comparisons to the Moon. In: Proceedings of the 2nd Moscow Solar Sytem Symposium. Absract 2MS3-MM-01.
Honda, C., Suzuki, S., Hirata, N., Morota, T., Demura, H., Ohtake M., Haruyama, J., Asada, N.., 2011. Retention time of crater ray materials on the Moon. American Geophysical Union, Fall Meeting 2011, abstract #P13D-1703.
Horz, F., Grieve, R., Heiken, G., Spudis, P., Binder, A., 1991. Lunar Surface Processes. In Lunar Source Book. A User's Guide to the Moon. Cambridge University Press, Cambridge, Great Britain, pp. 62–121.
Housen, K.R., Schmidt, R.M., Holsapple, K.A., 1983. Crater ejecta scaling laws: fundamental forms based on dimensional analysis. J. Geophys. Res. 88, 2485–2499.
Howard, K.A., 1972. Ejecta blankets of large craters exemplified by King crater. In: Apollo 16 Preliminary Science Report. NASA-SP-315 29–70, 29–781.
Ivanov, B.A., 2001. Mars/Moon cratering rate ratio estimates. Space Sci. Rev. 96, 87–104.
Karachevtseva, I., Oberst, J., Shingareva, K., Konopikhin, A., Nadejdina, I., Zubarev, A., Willner, K., Mut, N., Waehlisch, M., 2012. Global Phobos geodatabase and GIS analyses. LPSC-43, abs. # 1342.
Karachevtseva, Oberst, Zubarev, Nadezhdina, Kokhanov, Garov, Uchaev, Dm.V., Malinnikov and Klimkin, The Phobos information system, Planet. Space Sci. http://dx.doi.org/10.1016/j.pss.2013.12.015, in press.
Keil, K., 2002. Geologic history of asteroid 4 Vesta. In: Bottke, W.F., et al. (Eds.), Asteroids III. The University of Arizona Press, pp. 573–584.
Kleinhans, M.G., Markies, H., de Vet, S.J., Veld, A.C., Postema, F.N., 2011. Static and dynamic angles of repose in loose granular materials under reduced gravity. J. Geophys. Res. 116, E11004, http://dx.doi.org/10.1029/2011JE003865.
Kokhanov, A.A., Basilevsky, A.T., Karachevtseva, I.P., Nadezhdina, I.E., Zubarev, A.E., 2013. Depth/diameter ratio and inner wall steepness of large Phobos craters. LPSC-44, abs. #2289.
Kreslavsky, M.A., Head, J.W., 2012. New observational evidence of global seismic effects of basin-forming impacts on the Moon from Lunar Reconnaissance Orbiter Lunar Orbiter Laser Altimeter data. Journal of Geophysical Research 117, http://dx.doi.org/10.1029/2011JE003975 (E00H24).
Ksanfomality, L.V., Moroz, V.I., Bibring, J.P., Combes, M., Soufflot, A., Ganpantzerova, O.F., Goroshkova, N.V., Zharkov, A.V., Nikitin, G.E., Petrova, E.V., 1989. Spatial variations in thermal and albedo properties of the surface of Phobos. Nature 341, 588–591.
Kulander, B.R., Barton, C.C., Dean, S.L., 1979. The application of fractography to core and outcrop fracture investigations. U.S. Dept. Energy. METC/SP-79/3. National Tech. Inf. Service. U.S. Dept. of Commerce, Springfield, VA.
Lachenbruch, A.H., 1962. Mechanics of thermal contraction cracks and ice-wedge polygons in permafrost. Geol. Soc. Amer. Spec 70, 69.
Lee, P., 2009. In Proceedings of the First International Conference on the Exploration of Phobos and Deimos, 5–7 Nov 2007: Summary and Recommendations. Mars Inst. Tech. Pub. 2009–001, pp. 6–7.
Masursky, H., Batson, R.M., McCauley, J.F., 1972. 28 c-authors, 1972. Mariner 9 television reconnaissance of Mars and its satellites: preliminary results. Science 175, 294–305.
Melosh, H.J., 1989. Impact Cratering: A Geologic Process. Oxford Monographs on Geology and Geophysics. No 11. Oxford Univ. Press, New York, Clarendon Press, Oxford.
Morris, EC, Shoemaker, E.M., 1968. Craters. In: Surveyor Project Final Report Part II, Science results. TR 32-1265. JPL, Pasadena, 65–68.
Muehlberger, W.R., Batson, R.M., Boudette, E.L., 30 other coauthors. Preliminary geologic investigation of the Apollo 16 landing site. In: Apollo 16 Preliminary Science Report. NASA-SP-315, 1972 6-1-7-1.
Murchie, S., Erard, S., 1996. Spectral properties and heterogeneity of Phobos from measurements by Phobos 2. Icarus 123, 63–86.
Murchie, S.L., Britt, D.T., Head, J.W., et al., 1991. Color heterogeneity of the surface of Phobos: relationships to geologic features and comparison to meteorite analogs. J. Geophys. Res. 96 (N B4), 5925–5945.
Murchie, S.L., Thomas, N., Britt, D., et al., 1999. Mars pathfinder spectral measurements of Phobos and Deimos: comparison with previous data. J. Geophys. Res. 104 (N E4), 9069–9079.
Murray, J.B., Heggie, D.C., 2014. Character and origin of Phobos' grooves, Planetary and Space Science 102, 119–143.
Murray, J.B., Iliffe, J.C., Muller, J-P.A.L., Neukum, G., Werner, S., Balme, M., 2006. the HRSC Co-investigator team, 2006. New evidence on the origins of Phobos' parallel grooves from HRSC Mars Express. LPSC-37, abs. #2195.
Murray, J.B., Rothery, D.A., Thornhill, G.D., Muller, J.-P., Iliffe, J.C., Day, T., Cook, A.C., 1994. The origin of Phobos' grooves and crater chains. Planet. Space Sci.. 42, 512–526.
Murray, J.B., Iliffe, J.C., 2011. Morphological and geographical evidence for the origin of Phobos' grooves from HRSC Mars Express images. Geological Society, 356. Special Publications, London, pp. S21–S41.
Noland, M., Veverka, J., Pollack, J.B., 1973. Mariner 9 polarimetry of Phobos and Deimos. Icarus 20, 490–499.
Oberst, J., Zubarev, A., Nadejdina, I., Rambaux, N., 2014. Phobos control point network and rotation. Planet. Space Sci. 102, 45–50.
Pieters, C.M., Murchie, S.L., Thomas, N., Britt, D.T., 2014. Composition of surface materials on the moons of Mars. Planet. Space Sci. 102, 144–151.
Pohlman, N., Severson, B., Ottino, J., Lueptow, R., 2006. Surface roughness effects in granular matter: Influence on angle of repose and the absence of segregation. Phys. Rev. E 73 (031), 304.
Pollack, J.B., Burns, J.A., 1977. An origin by capture for the Martian satellites? Bull. Am. Astron.Soc. 9, 518–519.
Pollack, J.B., Veverka, J., Noland, M., 1973. Mariner 9 television observations of Phobos and Deimos. J. Geophys. Res. 78, 4313–4326.
Pronin, A.A., Nikolaeva, O.V., 1982. Dark halos of the Phobos craters and shock reproduction of carbon chondrites. Doklady Akad. Nauk SSSR 265, 429–432.
Quaide, W.L., Oberbeck, V.R., 1968. Thickness determinations of the lunar surface layer from lunar impact craters. J. Geophys. Res. 73, 5247–5270.
Ramsley, K.R., Head, J.W., 2013a. Mars impact ejecta in the regolith of Phobos: bulk concentration and distribution. Planet. Space Sci. 87, 115–129.
Ramsley, K.R., Head, J.W., 2013b. The origin of Phobos grooves from ejecta launched from impact craters on Mars: tests of the hypothesis. Planet. Space Sci. 75, 69–95.
Ramsley, K.R., Head, J.W., 2014. Constraints on the age of Stickney crater and associated features on Phobos. LPSC-45, abs. #1414.
Robinson, M.S., Thomas, P.C., Veverka, J., 2003. Missing craters on Eros, Phobos, and the Moon—crater erasure in a thick regolith? LPSC-34, abs. #1696.pdf.
Sagdeev, R.Z., Zakharov, A.V., 1989. Brief history of the Phobos mission. Nature 341, 581–585.
Schmedemann, N., Michael, G., Ivanov, B.A., Murray, J., Neukum, G., 2014. Surface chronology of Phobos: the age of Phobos and its largest crater, Stickney. Planet. Space Sci. 102, 152–163.
Shevchenko, V.V., Pine, P.K., Shevrel, S.D., Dadu, I., Lu, Y., Skobeleva, T.P., Kvaratskhelia, O., Rosemberg, K., 2012. Modern slope processes on the Moon. Sol. Syst. Res. 46 (no. 1), 1–17.
Shingareva, T.V., Basilevsky, A.T., Shashkina, V.P., et al., 2008. Morphological characteristics of the Phobos craters and grooves. LPSC-39, abs. #2425.
Shingareva, T.V., Kuzmin, R.O., 2001. Mass-wasting processes on the surface of Phobos. Sol. Syst. Res. 35, 431–443.

Shkuratov, Yu, G., Opanasenko, N.V., Basilevsky, A.T., et al., 1991. A possible interpretation of bright features on the surface of Phobos. Planet. Space Sci. 39, 341–347 (no. 1/2).
Shkuratov, Y.u., Kaydash, V., Videen, G., 2012. The lunar crater Giordano Bruno as seen with optical roughness imagery. Icarus 218, 525–533.
Shoemaker E.M., Morris E.C., 1969. Size-frequency distribution of fragmental debris. In: Surveyor Program Results. NASA SP-184. NASA. Washington, D.C. pp. 82–96.
Shuvalov, V.V., 2012. A mechanism for the production of crater rays. Meteorit. Planet. Sci. 47 (Suppl. 2), S262–S267.
Singer, K.N., McKinnon, W.B., Schenk, P.M., Moore, J.M., 2012. Massive ice avalanches on Iapetus mobilized by friction reduction during flash heating. Nat. Geosci. 5, 574–578.
Soter, S., Harris, A., 1977. Are striations on Phobosw evidence for tidal stress. Nature 268, 421–422.
Squyres, S.W., Clifford, S.M., Kuzmin, R.O., Zimbelman, J.R., Costard, F.M., 1992. Ice in the martian regolith. In: Kieffer, Mars. H.H., et al. (Eds.), 1992. University of Arizona Press, pp. 523–554.
Thomas, P., 1979. Surface features of Phobos and Deimos. Icarus 40, 223–243.
Thomas, P.C., 1993. Gravity, tides, and topography on small satellites and asteroids: Application to surface features of Martian satellites. Icarus 105, 326–344.
Thomas, P.C., 1998. Ejecta emplacement on the Martian satellites. Icarus 131, 78–106.
Thomas, P., Prockter, L., 2010. Tectonics of small bodies. In: Watters, T.R., Schultz, R. A. (Eds.), Planetary Tectonics. Cambridge University Press, pp. 233–263.
Thomas, P., Veverka, J., 1980. Downslope movement of material on Deimos. Icarus 42, 234–250.
Thomas, P.C., Veverka, J., Duxbury, T.C., 1978. Origin of the grooves on Phobos. Nature 273, 282–284.
Thomas, P.C., Veverka, J., Bloom, A., Duxbury, T.C., 1979. Grooves on Phobos: their distribution, morphology and possible origin. J. Geophys. Res. 84 (B14), 8457–8477.
Thomas, N., Barbieri, C., Keller, H.U., 2012. 27 coauthors, 2012. The geomorphology of (21) Lutetia: Results from the OSIRIS imaging system onboard ESA's Rosetta spacecraft. Planet. Space Sci. 66 (Issue 1), 96–124.
Thomas, N., Stelter, R., Ivanov, A., Bridges, N.T., Herkenhoff, K.E., McEwen, A.S., 2011. Spectral heterogeneity on Phobos and Deimos: HiRISE observations and comparisons to Mars Pathfinder results. Planet. Space Sci. 59, 1281–1292.
Trask, N.J., 1966. Size and spatial distribution of craters estimated from Ranger photographs. In: JPL TR 32-800, pp. 249–338.
Veverka, J., Duxbury, T.C., 1977. Viking observations of Phobos and Deimos: preliminary results. J. Geophys. Res. 82, 4213–4223.
Veverka, J.P., Thomas, P., Johnson, T.V., Matson, D., Housen, K., 1986. The physical characteristics of satellite surfaces. In: Burns, J.A., Matthews, M.S. (Eds.), Sattelites. Unoiv. Arizona Press, Tucson, pp. 342–402.
Waehlisch, M., Willner, K., Oberst, J., et al., 2010. A new topographic image atlas of Phobos. Earth Planet. Sci. Lett. 294 (Suppl. 3–4), 547–553.
Weidenschilling, S.J., 1979. A possible origin for the grooves of Phobos. Nature 282, 697–698.
Willner, K., Oberst, J., Hussmann, H., et al., 2010. Phobos control point network, rotation, and shape. Earth Planet. Sci. Lett. 294, 541–546.
Willner, K., Shi, X., Oberst, J., 2014. Phobos shape and topography models. Planet. Space Sci. 102, 51–59.
Wilson, L., Head, J.W., 2002. Tharsis-radial graben systems as the surface manifestation of plume-related dike intrusion complexes: models and implications. J. Geophys. Res. 107 (E8, 5037, 10.1029/2001JE001593).
Wilson, L., Head, J.W., 2014. Groove formation on Phobos: testing the Stickney ejecta emplacement model for a subset of the groove population. Planet. Space Sci. (in review).
Zubarev, A.E., Nadezhdina, I.E., Konopikhin, A.A., 2012. Problems of Processing of Remote Sensing Data for Modeling Shapes of Small Bodies in the Solar System. Modern Problems of Remote Sensing of the Earth from Space. Space Research Institute, Moscow, pp. 277–285 (in Russian).